European Commission
Information Society and Media

SEVENTH FRAMEWORK PROGRAMME

Network of Excellence

NEWCOM#

Network of Excellence in Wireless Communications#

FP7 Contract Number: 318306

WP2.1 – Radio interfaces for next generation wireless systems

D21.3
Analysis of initial results at EuWIN@CTTC

Contractual Delivery Date:	October 31, 2014
Actual Delivery Date:	November 21, 2014
Responsible Beneficiary:	CTTC
Contributing Beneficiaries:	CTTC, CTTC/UPC, CNIT/UniBo, CNIT/Torino, Bilkent, PUT, UCL, CNRS/Eurecom, AAU, CNRS/Satie
Estimated Person Months:	24
Dissemination Level:	Public
Nature:	Report
Version:	1.0

This page is left blank intentionally

Document Information

Document ID:	D21.3
Version Date:	Nov 18, 2014
Total Number of Pages:	68
Abstract:	The nature of this Deliverable of WP2.1 ("Radio interfaces for next-generation wireless systems") is mainly descriptive and its purpose is to provide a report on the status of the different Joint Research Activities (JRAs) currently ongoing, some of them being performed on the facilities that are available at EuWIn.
Keywords:	The main topics addressed are the need for more (efficient use of the) spectrum, channel modelling and performance evaluation of wireless systems, high data rates, and indoor location.

Authors

IMPORTANT: The information in the following two tables will be directly used for the MPA (Monitoring Partner Activity) procedure. Upon finalisation of the deliverable, please, ensure it is accurate. Use multiple pages if needed. Besides, please, adhere to the following rules:

- Beneficiary/Organisation: For multi-party beneficiaries (CNIT) and beneficiaries with Third Parties (CNRS and CTTC), please, indicate beneficiary *and* organisation (e.g., CNIT/Pisa, CNRS/Supelec).
- Role: Please, specify: Overall Editor / Section Editor / Contributor.

Full Name	Beneficiary / Organisation	e-mail	Role
Carles Fernández-Prades	CTTC	carles.fernandez@cttc.cat	Editor, Contributor
Guido Masera	CNIT/Polito	guido.masera@polito.it	Contributor
Davide Dardari	CNIT/UniBO	davide.dardari@unibo.it	Contributor
Giacomo Calanchi	CNIT/UniBO	giacomocalanchi@gmail.com	Contributor
Anna Umbert	UPC	annau@tsc.upc.edu	Contributor
Jordi Pérez Romero	UPC	jordip@xaloc.upc.edu	Contributor
Adrian Kliks	PUT	akliks@et.put.poznan.pl	Contributor
Paweł Kryszkiewicz	PUT	pkrysz@et.put.poznan.pl	Contributor
Ferran Casadevall	UPC	ferranc@tsc.upc.edu	Contributor
Pau Closas	CTTC	pclosas@cttc.cat	Contributor
Ana Moragrega	CTTC	amoragrega@cttc.cat	Contributor
Javier Arribas	CTTC	jarribas@cttc.cat	Contributor
Nikolaos Bartzoudis	CTTC	nikolaos.bartzoudis@cttc.es	Contributor
Oriol Font-Bach	CTTC	oriol.font@cttc.cat	Contributor
Miquel Payaró	CTTC	mpayaro@cttc.cat	Contributor
Evgenii Vinogradov	UCL	evgenii.vinogradov@uclouvain.be	Contributor
Claude Oestges	UCL	claude.oestges@uclouvain.be	Contributor
Wout Joseph	UGent	Wout.Joseph@intec.ugent.be	Contributor

Brecht Hanssens	UGent	Brecht.Hanssens@intec.ugent.be	Contributor
Vittorio Degli-Esposti	CNIT/UniBO	v.degliesposti@unibo.it	Contributor
Enrico Vitucci	CNIT/UniBO	enricomaria.vitucci@unibo.it	Contributor
Bernard Fleury	AAU	bfl@es.aau.dk	Contributor
Thomas Zemen	FTW	thomas.zemen@ftw.at	Contributor
Mingming Gan	FTW	gan@ftw.at	Contributor
Pawel Kryszkiewicz	PUT	pkrysz@et.put.poznan.pl	Contributor
Amor Nafkha	SUPELEC	Amor.NAFKHA@supelec.fr	Contributor

Reviewers

Full Name	Beneficiary / Organisation	e-mail	Date
Roberto Verdone	CNIT/UniBO	roberto.verdone@unibo.it	10/11/2014
Marco Luise	CNIT/UniPI	marco.luise@cnit.it	17/11/2014

Version history

Issue	Date of Issue	Comments
0.1	July 22, 2014	TOC definition – C. Fernández
0.2	September 3, 2014	First draft – C. Fernández
0.3	September 25, 2014	Second draft – C. Fernández
0.4	November 18, 2014	Final draft – R. Verdone
1.0	November 18, 2014	Final draft – M.Luise

Executive Summary

The nature of this Deliverable of WP2.1 (“Radio interfaces for next-generation wireless systems”) is mainly descriptive and its purpose is to provide a report on the status of the different Joint Research Activities (JRAs) currently ongoing, some of them being performed on the facilities that are available at EuWIn. As it is shown along the document, there is already an important flow of achievements that are emerging from those activities, materialized in a number of joint papers and knowledge transfer to the industry. The main topics addressed are the need for more (efficient use of the) spectrum, channel modelling and performance evaluation of wireless systems, high data rates, and indoor location.

Annex I provides details about the JRA results. Annex II and III are in common to D22.3 and D23.3 and are not reported here (see D22.3).

Table of Contents

1. Introduction

The Joint Research Activities (JRAs) described in this document address those challenges identified as key issues in the development of radio interfaces for the Future Internet, such as the need for more (efficient use of the) spectrum, channel modelling and performance evaluation of wireless systems, high data rates, and indoor location. The list of main achievements after the second year of NEWCOM# is the following:

- ✓ **JRA #A - Enhanced NC-OFDM transmission with reduced spurious emission level (PUT + CNRS/SUPELEC)**
  The aim of this JRA is to decrease power consumption and increase spectral efficiency of NC-OFDM transmitter. The power consumption can be decreased by reducing computational complexity in a transceiver and increasing energy efficiency of power amplifier. It means that algorithms "enhancing" NC-OFDM operation have to be low computationally complex. On the other hand, modelling of practical power amplifier has to be carried out in order to efficiently reverse the nonlinearity effect and calculate its energy efficiency. An algorithm for reduction of both intermodulation and subcarrier spectrum side lobes has been proposed, exhibiting low computational complexity, as well as an enhanced version that makes use of the context information on the Primary Users, that can improve spectrum shaping performance.

- ✓ **JRA #B - Practical implementation of polar codes (CNIT/Polito + BILKENT + CTTC)**
  This activity is focused on the VLSI implementation of the Belief Propagation (BP) algorithm applied to the decoding of Polar Codes. A first BP decoding architecture has already been developed and synthesized to have a preliminary comparison with respect to alternative decoding approaches and codes. Notwithstanding the different clock frequencies, BP decoder achieves a higher throughput than Successive Cancellation (SC) decoding, confirming that BP decoding is a promising approach to target high throughput applications. In terms of occupied area, the BP decoder is larger than both SC solution and a fully parallel LDPC decoder. This difference can be reduced by means of specific optimizations in the architecture design.

- ✓ **JRA #C - Assessment and development of multi-link channel model (UCL + Ugent (Associate Partner Type II) + CNIT/UniBO + AAU + FTW)**
  This JRA aims at developing to and experimentally validating accurate and computationally effective multi-link channel models applicable to cooperative and interference-limited networks. Regarding the assessment, a draft of the review paper has been circulated among partners and is under revision by the partners. The plan is to pursue and finalize this activity in the next period. Regarding the development of channel models, three activities are currently on-going: *i*) Development of indoor multi-link channel models (UCL, UGent): a first model was designed and the resulting submitted paper is now in revision. It is now being extended to include angular properties, as well combined with room-electromagnetic theory to include late components. This model also serves as a basis for interaction with JRA-H. A joint UCL-UGent experimental campaign was carried out in February 2014 to estimate the channel dynamics in various indoor environments. Measurement results are currently being analysed; *ii*) Dense multipath depolarization modelling: the polarimetric properties of so-called Dense Multipath Components were investigated in various outdoor and indoor environments, relying on broadband measurements and Ray-Tracing simulations; and *iii*) Extended ray-tracing modelling for UWB transmissions: an existing ray-tracing tool is being extended with UWB capability.

- ✓ **JRA #F - Design and experimental validation of algorithms for active and passive indoor positioning (CTTC + CNIT/UNIBO, joint activity WP2.1 and WP2.2)**
  The purpose of this JRA is to perform a practical approach to indoor positioning. After a survey of the current available technologies for indoor positioning, researchers have

continued the development of an open, reliable and modular system for testing several technologies and collect the data measurements, as well as the development of algorithms for indoor positioning exploiting data fusion between WiFi RSS and inertial measurements. During this period, a robotic platform has been developed in order to provide repeatability in the experiments performed in real-life environments.

- ✓ **JRA #G - Spectrum occupancy measurements and database exploitation (PUT + UPC)**
  The purpose of this JRA is to make spectrum measurements to assess the spectrum availability for cognitive radio. Several frequency bands from 200 MHz up to 3 GHz have been monitored up to date in the two sites, both Poznan and Barcelona. Obtained results show significant amounts of unused spectrum, with similar results for both sites when analysed globally (average spectrum occupancy of 27% in Poznan and 22% in Barcelona). On the contrary, when going to the detailed analysis of some specific bands, more relevant differences are obtained. These differences have been observed mainly in the Terrestrial TRunked RAdio (TETRA) bands that in Poland are also used by Code Division Multiple Access (CDMA) 450, as well as in the bands of the Global System for Mobile communications (GSM) due to the effects of Universal Mobile Telecommunications System (UMTS) refarming in the 900 MHz band.

- ✓ **JRA #H - Impact of channel model in the performance evaluation of wireless systems (CTTC + UCL)**
  The principal goal of this JRA is to experimentally analyse the impact that different channels (channel models) have on the performance of modern wireless communication systems. Towards this end, it has been deployed a complex laboratory setup comprising a real-time FPGA-based PHY-layer prototype, of an LTE-based macrocell/femtocell interference-mitigation scheme composed by i) a single macro base station (BS) and user equipment (UE) pair representing the primary downlink (DL) communication link, ii) a single femto BS and UE pair representing a secondary DL communication link (which makes use of an opportunistic frequency-reuse scheme and therefore features adaptive subcarrier allocation to avoid interfering the primary link) and iii) a real-time multi-channel emulator with capacity to provide both static and mobile channel conditions (i.e., for standard and custom channel models), as well as allowing to reproduce the desired interference scenarios in a controlled lab environment. Based on this hardware setup initial actions were made to evaluate the performance of the real-time LTE-based interference-mitigation scheme under realistic operating conditions. The evaluation was comprehensive enough to validate the impact that different channel models (i.e., ITU Pedestrian B and 3GPP Extended Pedestrian A, at different speeds) have on the effectiveness of the evaluated interference-mitigation scheme and, ultimately, on the performance observed for the primary communication link.

1.1 Glossary

ADC	Analog-to-digital converter
BER	Bit Error Rate
BP	Belief Propagation
BS	Base Station
CDMA	Code Division Multiple Access
CIR	Channel impulse response
DVB-T	Digital Video Broadcasting – Terrestrial
FPGA	Field Programmable Gate Array
GSM	*Global System for Mobile* communications
JRA	Joint Research Action
LDPC	Low-Density Parity-Check
LTE-A	Long Term Evolution – Advanced
NC-OFDM	Non-Contiguous Orthogonal Frequency Division Multiplexing
PHY	Physical layer
REM	Radio Environmental Map
RSS	Received Signal Strength
RX	Receiver
SC	Successive Cancellation
SNIR	Signal to Noise plus Interference Ratio
SNR	Signal Noise Ratio
TVWS	TeleVision White Spaces
UE	User Equipment
UMTS	*Universal Mobile Telecommunications System*
USRP	Universal Software Radio Peripheral
VLSI	Very Large Scale Integration

2. Joint Research Activities

This Section describes the activities within WP 2.1 carried out in the second year of the project.

2.1 JRA#A - Enhanced NC-OFDM transmission with reduced spurious emission level

2.1.1 Participant researchers and affiliations

- Pawel Kryszkiewicz – PUT
- Amor Nafka – CNRS/SUPELEC

2.1.2 Description

The aim of this JRA is to decrease power consumption and increase spectral efficiency of NC-OFDM transmitters. The power consumption can be decreased by reducing computational complexity in a transceiver and increasing energy efficiency of power amplifier. It means that algorithms “enhancing” NC-OFDM operation have to be low computationally complex. It is therefore connected with algorithms designed in Track 1, within JRA on Advanced filtering and adaptive signal processing. On the other hand, modelling of practical power amplifiers has to be carried out in order to efficiently reverse the nonlinearity effect and calculate its energy efficiency. These measurements can be made using USRP platform as it is a part of equipment used by both PUT and CNRS/SUPELEC.

2.1.3 Relevance with the identified fundamental open issues

This JRA is relevant to tasks 2.1.2 Low-energy-consumption and low-emission radio interfaces and 2.1.4 High spectrally-efficient radio interfaces. It aims at reduction of energy consumption of the radio transmitter thanks to improvement of the modulation scheme and consideration of nonlinear effects. Additionally, NC-OFDM improves spectral efficiency thanks to utilization of frequencies close to others systems.

2.1.4 Initial results

Initially, in connection to Track 1, an algorithm for reduction of both intermodulation and subcarrier spectrum sidelobes was proposed by us in [1]. It has low computational complexity, similarly as the other algorithm proposed in [2] that makes use of the context information on the Primary Users that can improve spectrum shaping performance. Although both algorithms could be evaluated directly on the USRP hardware, it would be reasonable to first model the nonlinearity of power amplifier used in the USRP. Two possibilities for USRP power amplifier characteristic calculation were considered: by built-in internal RX path in USRP device, and by external high-class device, i.e. Rohde&Schwarz FSL Spectrum Analyzer in IQ trace setup. The characteristic seems to be quasi-memoryless, so modelling using polynomial with complex coefficients is possible.

2.1.5 Achievements and planned activities

Achievements:

- Proposal of low complex algorithms for NC-OFDM spectrum shaping
- Investigation of possibilities and measurement of USRP nonlinearity characteristic

Planned activities:

- Predistortion of transmitted signal to confirm in “in-direct” manner correctness of considered model
- Reduction of both subcarrier spectrum sidelobes and intermodulation evaluated in a real hardware.

2.1.6 Publications

[1] Pawel Kryszkiewicz, Adrian Kliks, Yves Louet " Reduction of subcarriers spectrum sidelobes and intermodulation in NC-OFDM systems " WiMOB 2013, October 2013, Lyon, France

[2] Pawel Kryszkiewicz, Hanna Bogucka "Advanced Interference Reduction in NC-OFDM Based Cognitive Radio with Cancellation Carriers" EUSIPCO 2014, September 2014, Lisbon, Portugal

2.2 JRA#B - Practical implementation of polar codes

2.2.1 Participant researchers and affiliations

Institutions and researchers involved in the Polar Code activities are:

- CNIT/Polito (Guido Masera, Andrea Biroli, Maurizio Martina)
- Bilkent University (Erdal Arikan)
- CTTC (Luis Blanco)

More precisely, Bilkent University provides support on software modelling, codes, optimization of the decoding algorithm; CNIT/Polito operates on bit and cycle accurate software models, architecture design and development of synthesizable hardware models; CTTC makes available their hardware platform to evaluate BER performance of addressed codes on real operation channels.

2.2.2 Description

The planned activity is focused on the VLSI implementation of the Belief Propagation (BP) Algorithm applied to the decoding of Polar Codes. Cooperation between Bilkent University and CNIT/Polito is mainly based on two exchanges:

- PhD student Andrea Biroli will work a six months period of work in Ankara, to complete and refine the software model of the BP decoder, and to develop a fully synthesizable hardware model. The student moved to Bilkent in May and he is currently working at the hardware design.
- A second researcher will move to Torino in October, to closely work with the Polito group at the hardware synthesis.

In this cooperation, Bilkent provides expertise on Polar code design, decoding algorithm and software modeling, while Polito exploits its knowledge and skills in the hardware modeling and VLSI architecture design of communication systems.

2.2.3 Relevance with the identified fundamental open issues

The joint work led to a number of relevant conclusions that are now driving the modeling activity:

- Manufacturing companies require decoding architectures with performance that goes towards 1 to 10 Gb/s for throughput and 1nJ/b to 10 pJ/b for energy consumption.
- Current implementations of Successive Cancellation (SC decoding) can reach throughput of 40 Mb/s on a FPGA devices. Also consumptions are in the order of 10 nJ/b.
- Since one decision at each clock cycle is taken and many data dependencies exist in the algorithm, SC decoding is strictly limited by the working frequency (clock rate).
- On the other side, BP decoding can take more than one decision at each clock cycle (higher potential parallelism) so BP can be proposed to enhance throughput speed and reduce decoding latency.

Based on these conclusions, the Bilkent/CNIT cooperation will proceed towards the following objectives:

- To refine BP decoding and to provide a number of possible architectural improvements
- To develop SW/HW models for the identified architectural solutions (and for new modified polar codes) in order to compare performance and complexity
- Complexity comparison between BP and SC in terms of throughput, area and energy
- To embed adaptive techniques and stopping algorithms
- To fully characterize a final ASIC and FPGA implementation

The activity is also extended to CTTC for the performance evaluation of PC and related decoding algorithms on real hardware platforms, which include RF front-ends and real wireless channel.

2.2.4 Initial results

A first BP decoding architecture has already been developed and synthesized to have a preliminary comparison with respect to alternative decoding approaches and codes. Table 1 shows the obtained results and the comparisons with two different decoder implementations.
Comparisons are given with respect to a SC decoder and an LDPC decoder:

[1]:Fully parallel decoder, A. Blanksby and C. Howland, “A 690-mw 1-gb/s 1024-b, rate-1/2 low density parity-check code decoder,” Solid-State Circuits, IEEE Journal of, vol. 37, no. 3, pp. 404 –412, mar 2002.

[2]:SC-based decoder, C. Leroux, A. Raymond, G. Sarkis, and W. Gross, “A semi-parallel successive-cancellation decoder for polar codes,” Signal Processing, IEEE Transactions on, vol. PP, no. 99, p. 1, 2012

It can be noticed that, notwithstanding the different clock frequencies, BP decoder achieves a higher throughput than SC: this confirms that BP decoding is a promising approach to target high throughput applications. In terms of occupied area, the BP decoder is larger than both SC solution and a fully parallel LDPC decoder. This difference can be reduced by means of specific optimizations in the architecture design.

	[1]	[2]	This Work
Code	LDPC	Polar code	Polar code
Codelength	1024	1024	1024
Rate	1/2	1/2	1/2
N. of Iterations	64	-	10
Technology	160 nm	65 nm	90 nm
Quantization	4	6	8
Clock Frequency	64 MHz	500 MHz	200 MHz
Core Area	2.9 mm^2	0.35 mm^2	2.79 mm^2
Normalized Area @ 90 nm	0.92 mm^2	0.67 mm^2	2.79 mm^2
Throughput	1 Gb/s	123 Mb/s	170 Mb/s
SNR $[@BER = 10^{-4}]$	2.7 dB	3.1 dB	2.3 dB

Table 1: Comparison between different decoder implementations

2.2.5 Publications

Results summarized in the previous section have been presented at the European Conference on Networks and Communications, held in Bologna, Italy, in June 2014:

Andrea Biroli, Guido Masera “A VLSI Implementation of the Belief Propagation Algorithm Applied to the Decoding of Polar Codes”, Special Session on “From Theory to Practice: Experimental Research Activities in NEWCOM#’s EUWIN Labs”, European Conference on Networks and Communications, held in Bologna, Italy, June 23/26, 2014

2.3 JRA#C - Assessment and development of multi-link channel model

2.3.1 Participant researchers and affiliations

Evgenii Vinogradov and Claude Oestges (UCL), Wout Joseph and Brecht Hanssens (Ugent – Associate Partner Type II), Vittorio Degli-Esposti and Enrico Vitucci (CNIT-UNIBO), Troels Perdersen and Bernard Fleury (AAU), Thomas Zemen and Mingming Gan (FTW).

2.3.2 Description

This JRA intends to develop and experimentally validate accurate and computationally effective multi-link channel models applicable to cooperative and interference-limited networks. The first aim is to assess the assets and deficiencies of existing cooperative and multi-link channel models, the objective being to publish a review paper in a magazine or journal. The second and main goal is to develop and experimentally validate representations of complex multi-dimensional radio channels for cooperative communications. These models shall then be included within EuWIN for channel emulations and performance simulations.

2.3.3 Relevance with the identified fundamental open issues

The multi-dimensional radio channel remains central in interference-limited scenarios. Multiple antenna systems, interference recognition and management as well as cooperation among separate network nodes are inherently multi-dimensional techniques and should always be designed with a proper knowledge not only of the channel, but also of the interference. Hence, a multi-dimensional description of the radio channel characteristics is required in order to exploit all these dimensions when designing transmission protocols. This is why some of the developed channel models will be included in the performance evaluation of JRA-H. Also, channel models will be developed in parallel to JRA-D to guarantee as much consistency as possible.

2.3.4 Achievements and planned activities

Regarding the assessment, a draft of the review paper has been circulated among partners and is under revision by the partners. The plan is to pursue and finalize this activity in the next period. Regarding the development of channel models, three activities are currently on-going.

- Development of indoor multi-link channel models (UCL, UGgent): a first model was designed and the resulting submitted paper is now in revision. It is now being extended to include angular proprties, as well combined with room-electromagnetic theory to include late components. This model also serves as a basis for interaction with JRA-H. A joint UCL-UGent experimental campaign was carried out in February 2014 to estimate the channel dynamics in various indoor environments. Measurement results are currently being analyzed.
- Dense multipath depolarization modeling (UCL, CNIT/UniBO): the polarimetric properties of so-called Dense Multipath Components were investigated in various outdoor and indoor environments, relying on broadband measurements and Ray-Tracing simulations.
- Extended ray-tracing modeling for UWB transmissions (UCL, FTW): an existing ray-tracing tool is being extended with UWB capability.

2.3.5 Publications

E. Vitucci, F. Mani, V. Degli-Esposti, C. Oestges, Dense multipath depolarization in outdoor and indoor radio transmissions, XXXIst General Assembly of International Union of Radio Science – URSI (Beijing, China), August 2014.

E. Vinogradov, W. Joseph, C. Oestges, Modeling and simulation of fast fading channels in indoor peer-to-peer scenarios, 8th European Conference on on Antennas and Propagation, EuCAP '14 (Den Haag, The Netherlands), April 2014.

E. Vinogradov, W. Joseph, C. Oestges, Measurement-based modeling of time-variant fading statistics in indoor peer-to-peer scenarios, *IEEE Trans. Ant. Propagat*. (submitted, in revision).

2.4 JRA#F - Design and experimental validation of algorithms for active and passive indoor positioning

2.4.1 Participant researchers and affiliations

- From CTTC: Carles Fernández Prades, Pau Closas, Javier Arribas, Ana Moragrega.
- From CNIT/UniBO: Davide Dardari, Giacomo Calanchi.
- External researchers: Hector Torres (Universidad Tecnológica Metropolitana – Chile)

2.4.2 Description

This JRA is being mainly carried out within OpenInLocation, the laboratory on indoor positioning at the Centre Tecnològic de Telecomunicacions de Catalunya (CTTC), which is part of the European Lab on Wireless Communications for the Future Internet (EuWIn). Its goal is to devise, design, develop and test indoor location solutions.

2.4.3 Relevance with the identified fundamental open issues

Indoor location is today a hot topic both from academia and commercial standpoints.

2.4.4 Initial results

(i) A survey of the current available technologies for indoor positioning;
(ii) The development of an open, reliable and modular system for testing several technologies and collect the data measurements;
(iii) The development of an algorithm for indoor positioning exploiting data fusion between WiFi RSS and inertial measurements.
(iv) Academic partners external to NEWCOM# are actively collaborating and contributing to the activity, consolidating the laboratory and opening oportunities for its continuity after NEWCOM#, one of the initial objectives of EuWIn Labs.

2.4.5 Achievements and planned activities

There is a working prototype consisting of a moving robot that houses a control board, inertial measurement devices, WiFi and Bluetooth interfaces. This platform is able to run data fusion algorithms for indoor location and provides repeatability in the experiments, hence allowing fair performance assessment. Next steps will consist of experimenting with different scenarios and configurations, including methods for rapid, low-cost on-site deployment.

2.4.6 Publications

These publications have specific acknowledgements to NEWCOM#:

- Xiaoli Liu, Muqing Liang, Yu Morton, Pau Closas, Ting Zhang, Zhigang Hong, “Performance evaluation of MSK and OFDM modulations for future GNSS signals”, GPS Solutions, April 2014, Volume 18, Issue 2, pp 163-175.
- Javier Arribas, Pau Closas, and Carles Fernández-Prades, “Interference Mitigation in GNSS Receivers by Array Signal Processing: A Software Radio Approach”, in Proceedings

of the 8th IEEE Sensor Array and Multichannel Signal Processing Workshop, June 22-25 2014, A Coruña (Spain).

- J. Vilà-Valls, Q. Wei, P. Closas, C. Fernández-Prades, “Robust Gaussian Sum Filtering with Unknown Noise Statistics: Application to Target Tracking”, in Proceedings of the IEEE Workshop on Statistical Signal Processing (SSP), 29-2 July 2014, Gold Coast (Australia).

2.5 JRA#G - Spectrum occupancy measurements and database exploitation

2.5.1 Participant researchers and affiliations

Adrian Kliks and Paweł Kryszkiewicz (PUT)

Jordi Pérez-Romero, Anna Umbert and Ferran Casadevall (UPC)

2.5.2 Description

The purpose of this JRA is to make spectrum measurements to identify the spectrum availability for cognitive radio. Several frequency bands from 200 MHz up to 3 GHz have been monitored up to date in the two sites, Poznan and Barcelona. The focus has been more on the TeleVision White Spaces (TVWS) band, identified as a candidate band to extend the capacity of cellular systems when considering small cell deployments. In this respect, measurements both in indoor and outdoor locations are being done with the objective of building a Radio Environmental Map (REM) database that can be used as a support for small cell deployment strategies in connection with JRA #A of WP1.3. The analysis of the stability and other important features of the observed spectrum occupancy in the context of indoor/outdoor REM is then being analysed.

2.5.3 Relevance with the identified fundamental open issues

As discussed in Deliverable D13.1 [1] the use of shared spectrum such as TVWS to extend the capacity in LTE and LTE-A networks has been found particularly relevant in different works [2]-[11] for small cell scenarios. However, there are actually still very few works that have addressed the problem of how to allocate TVWS spectrum in an optimized way. In this context, this activity intends to support the theoretical activities by analyzing in particular the characteristics of the TVWS band (e.g. stability, etc.) so that a REM database can be built. Moreover, the activity also addresses the design of the REM structure including the relevant parameters to be stored.

2.5.4 Initial results

A comparative study of two measurement campaigns carried out in Barcelona, Spain, and Poznan, Poland, is presented in [JRAG-P1] to identify spectrum occupancy in different bands. In both cases the measurement setup was harmonized to obtain comparable results. The problem of efficient noise floor estimation was also considered and a pragmatic approach that takes into account both internal and ambient noise has been proposed. Obtained results show significant amount of unused spectrum, with similar results for both sites when analysed globally (average spectrum occupancy of 27% in Poznan and 22% in Barcelona). On the contrary, when going to the detailed analysis of some specific bands, more relevant differences are obtained. These differences have been observed mainly in the Terrestrial TRunked RAdio (TETRA) bands that in Poland are also used by Code Division Multiple Access (CDMA) 450, as well as in the bands of the Global System for Mobile communications (GSM) due to the effects of Universal Mobile Telecommunications System (UMTS) refarming in the 900 MHz band.

In [JRAG-P2] an intensive indoor measurement campaign in two locations (Poznań, Poland and Barcelona, Spain) is presented and analyzed to investigate their potential in the generation of digital indoor REMs. The existence of such detailed and stable maps will allow for further definition of the allowed transmit power of small cell transceivers operating within indoor heterogeneous

networks and making use of TeleVision White Spaces (TVWS). The analysis concentrates on the stability and repeatability of the measured values both over time and location, as key elements enabling the creation of aforementioned digital maps.

In [JRAG-P3] the analysis of the spectrum occupancy in the TV band is provided based on the indoor and outdoor measurements campaigns carried out in Poznan, Poland, and Barcelona, Spain, in 2013. The goal of this work is to discuss the stability and other important features of the observed spectrum occupancy in the context of indoor/outdoor REM database deployment. Details of all these results are given in the Annex.

The structure of the REM database for computing the maximum allowed transmit powers not to interfere with TV receivers is presented in [JRAG-P4] based on real measurements. Results include the analysis of the spatial granularity and time stability of the measurements, and the maximum allowed transmit powers considering both co-channel and adjacent channel transmission, as well as the existence of other secondary transmitters. Results reveal that in the considered building small cell deployment using co-channel transmission is not feasible due to the very low resulting allowed transmit powers. However, when adjacent channel transmission is considered, the resulting maximum allowed power levels can be more adequate for successful small cells deployment (e.g. in half of the points inside the building the transmit power can be higher than –6 dBm in the first adjacent channel). Details of these results are given in Annex 4.7.

We have also analysed different spectrum sensing methods able to detect primary users at low SNR levels. In that sense, in [JRAG-P5] we proposed a method based on the cyclic prefix (CP) of OFDM symbol and we compare it with the well-known energy detector. We concluded that the simple energy detection does not provide sufficient efficiency since for quite number of observed samples (one OFDM symbols) and perfect knowledge of the noise variance the primary user signal can be detected at SNR around -15dB achieving probability of detection around 0.9. Although similar results can be obtained for the proposed CP-based method it has to be highlighted that the real accuracy of the energy detector will be much worse due to the inaccuracy of the noise variance estimation. It further means that the application of the feature-detection based spectrum sensing methods for signal detection should be applied in low-SNR regimes which are characteristic for the indoor environments. Moreover, the CP-based method offers a quite reliable method for SNR estimate that can be used as additional information stored in the indoor REMs.

Finally in [JRAG-P6] we extended the measurements campaigns with street drive-tests and compared with the indoor measurements done in Poznan and Barcelona, focusing on the similarities and differences that occur between indoor measurements and drive tests.

2.5.5 Achievements and planned activities

Summary of achievements:

- Comparison of spectrum occupancy measurements in multiple bands carried out in two different cities, Barcelona (UPC) in Spain and Poznań (PUT) in Poland.
- Multiple indoor and outdoor spectrum occupation measurements are available, particularly in the TVWS band, but also in other bands.
- Indoor TVWS measurements have revealed that the received signal strength is quite stable during the daily usage of the building, and the main variance is observed as a function of the

location inside it. It can be concluded that it is feasible to construct a REM that will allow for reliable deployment of new transceivers inside the building and for coexistence of these systems.
- The structure of an indoor REM for supporting small cell deployment has been developed. Based on real measurements, this has allowed the computation of the maximum allowed power for small cells inside the building in order not to interfere the primary receivers.

Planned activity:

- Based on the available indoor measurements in one building future work includes the analysis of the impact towards DVB-T receivers located in other buildings close to the considered one, the analysis of other DVB-T channels and the optimisation of the maximum allowed transmit power when multiple small cells exist.

- Incorporate indoor measurements in a REM in the framework of the resource allocation in hetnets according to the research activities done in WP1.3 (JRA 1.3.3.A).

2.5.6 Publications

[JRAG-P1] A. Kliks, P. Kryszkiewicz, J. Pérez-Romero, A. Umbert, F. Casadevall, “Spectrum occupancy in big cities–comparative study”, ISWCS 2013 conference – Workshop on Cognitive Radio Advances, Applications and Future Emerging Technologies. August, 2013, Joint paper PUT/UPC.

[JRAG-P2] A. Kliks, P. Kryszkiewicz, A. Umbert, J.Pérez-Romero, F. Casadevall, “TVWS Indoor Measurements for HetNets”, IEEE WCNC 2014 - Workshop on Interference and Design Issues for Future Heterogeneous Networks, Istambul, 6th April, 2014. Joint paper PUT/UPC.

[JRAG-P3] A. Kliks, P. Kryszkiewicz, K. Cichon, A. Umbert, J.Pérez-Romero, F. Casadevall, "DVB-T channels power measurements in indoor/outdoor cases", ICTF conference, May, 2014, Joint paper PUT/UPC.

[JRAG-P4] A. Umbert, J.Pérez-Romero, F. Casadevall, A. Kliks, P. Kryszkiewicz, "On the use of Indoor Radio Environment Maps for HetNets Deployment", CROWNCOM conference, June, 2014, Joint paper PUT/UPC.

[JRAG-P5] P. Kryszkiewicz, A. Kliks, J.Pérez-Romero, A. Umbert, “DVB-T signal detection for indoor environments in low-SNR regime”, TELECOMMUNICATION REVIEW AND TELECOMMUNICATION NEWS, ISSN: 1230-3496, Journal of the Polish Society of Electrical Engineer. Accepted (to be published in September 2014).

[JRAG-P6] A. Kliks, P. Kryszkiewicz, K. Cichon, A. Umbert, J. Perez-Romero, F. Casadevall, “DVB-T channels measurements for the deployment of outdoor REM databases”, Journal of Telecommunications and Information Technology (JTIT), No. 3, 2014. Accepted (to be published in September 2014.

2.6 JRA#H - Impact of channel model in the performance evaluation of wireless systems

2.6.1 Participant researchers and affiliations

Miquel Payaró, Nikolaos Bartzoudis and Oriol Font-Bach (CTTC)
Claude Oestges and Evgenii Vinogradov (UCL)

2.6.2 Description

The principal goal of this JRA is to experimentally analyse the impact that different channel models have on the performance of modern wireless communication systems. Towards this end, it has been deployed a complex laboratory setup comprising the following entities:

- A real-time FPGA-based PHY-layer prototype, of a LTE-based macrocell/femtocell interference-mitigation scheme composed by four entities:
- A single macro base station (BS) and user equipment (UE) pair represent the primary downlink (DL) communication link.
- A single femto BS and UE pair represent a secondary DL communication link, which makes use of an opportunistic frequency-reuse scheme and therefore features adaptive subcarrier allocation to avoid interfering the primary link.
- A real-time multi-channel emulator with capacity to provide both static and mobile channel conditions (i.e., for standard and custom channel models), as well as allowing to reproduce the desired interference scenarios in a controlled lab environement.

Based on this hardware setup initial actions were made to evaluate the performance of the real-time LTE-based interference-mitigation scheme under realistic operating conditions. The present JRA has a strong link with JRA#C, which will provide different channel models to be loaded onto the channel emulator. Finally, a series of performance metrics (e.g., in the form of BER vs SINR curves) will be extracted for different operating conditions, providing an assessment of the impact that the considered channel models have on the performance of the system under test.

2.6.3 Relevance with the identified fundamental open issues

The validation and performance assessment of novel PHY-layer algorithms and technologies is typically limited to computer models and simulations. However the experimental validation which is not that common in academic research due to lack of resources, expertise and the high complexity involved, adds a top-up value to the developed PHY-layer technologies since:

- it brings a research idea closer to reality
    - e.g., account for implementation losses, signal impairments, non idealities, realistic mobility-interference and respective propagation channels
- addresses operational interdependencies in those technologies/algoorithms requiring real-time operation and validation
    - e.g., closed-loop schemes
- covers large periods of activity
    - e.g., thousands of frames for each value of the different operating parameters being considered

The mentioned factors pose important limitations when the target scenario is modelled and validated using a computer-based simulation environment. An effective way to overcome these

limitations is to develop a PHY-layer prototype capable of generating, receiving and processing the required signals in real-time.

2.6.4 Initial results

The above mentioned scenario has already been deployed and evaluated experimentally (see the publication section). During this initial performance-assessment stage it has been used a set of standard channels (i.e., including both static and mobile conditions).

2.6.5 Achievements and planned activities

The previously mentioned evaluation was comprehensive enough to validate the impact that different channel models (i.e., ITU Pedestrian B and 3GPP Extended Pedestrian A, at different speeds) have on the effectiveness of the evaluated interference-mitigation scheme and, ultimately, on the performance observed for the primary communication link. Nonetheless, a deeper evaluation is still required covering a more richer set of conditions (e.g., a single static custom channel was considered for the interfering signal). In this sense, the work will be extended to bring the operating conditions closer to the real-world (e.g., including the utilization of an indoor-to-outdoor channel for the interfering signal). This will allow to better characterize the impact of the considered channel model on the evaluation of the performance of a wireless communication scheme (i.e., a new measurement campaign will be performed using the channel models provided by JRA#C).

2.6.6 Publications

1. O. Font-Bach, N. Bartzoudis, A. Pascual Iserte, M. Payaró, L. Blanco, D. López Bueno and M. Molina, Interference Management in LTE-based HetNets: a Practical Approach, Transactions on Emerging Telecommunications Technologies, (available on-line, DOI: 10.1002/ett.2833; April 2014).
2. O. Font-Bach, N. Bartzoudis, M. Payaró and A. Pascual-Iserte, Measuring the performance of a distributed interference management scheme in a LTE-based HetNet deployment, (to appear) in Proceedings of the IEEE Sensor Array and Multichannel Signal Processing Workshop (SAM 2014), 22-25 June 2014, A Coruña (Spain).
3. N. Bartzoudis, O. Font-Bach, M. Payaró, A. Pascual-Iserte, J. Rubio, J. J. García Fernández and A. García Armada, Energy Profiling of FPGA-based PHY-layer Building Blocks Encountered in Modern Wireless Communication Systems, (to appear) in Proceedings of the IEEE Sensor Array and Multichannel Signal Processing Workshop (SAM 2014), 22-25 June 2014, A Coruña (Spain).
4. O. Font-Bach, N. Bartzoudis, M. Payaró and A. Pascual-Iserte, Hardware-efficient implementation of a Femtocell/Macrocell interference-mitigation technique for high-performance LTE-based systems, in Proceedings of the International Conference on Field Programmable Logic and Applications (FPL 2013), 2-4 September 2013, Porto (Portugal).

3. Conclusions

The Joint Research Activities (JRAs) described in this document are addressing those challenges identified as key issues in the development radio interfaces for the Future Internet, such as the need for more (efficient use of the) spectrum, channel modelling and performance evaluation of wireless systems, high data rates, and indoor location.

Regarding spectral occupancy, the main achievements are the proposal of low complex algorithms for NC-OFDM spectrum shaping and the investigation of possibilities and measurement of USRP nonlinearity characteristic. This research will continue analysing predistortion of transmitted signal to confirm in “in-direct” manner correctness of considered model, as well as the reduction of both subcarrier spectrum sidelobes and intermodulation evaluated in a real hardware.

Regarding spectrum occupation measurements and database exploitation, a comparison of spectrum occupancy measurements in multiple bands have been carried out in two different cities, Barcelona (UPC) in Spain and Poznań (PUT) in Poland, revealing that multiple indoor and outdoor spectrum occupation measurements are available, particularly in the TVWS band, but also in other bands. Indoor TVWS measurements have revealed that the received signal strength is quite stable during the daily usage of the building, and the main variance is observed as a function of the location inside it. It can be concluded that it is feasible to construct a REM that will allow for reliable deployment of new transceivers inside the building and for coexistence of these systems. The structure of an indoor REM for supporting small cell deployment has been developed as well. Based on real measurements, this has allowed the computation of the maximum allowed power for small cells inside the building in order not to interfere the primary receivers. In this sense, planned activities will address the analysis of the impact towards DVB-T receivers located in other buildings close to the considered one, the analysis of other DVB-T channels and the optimisation of the maximum allowed transmit power when multiple small cells exist, and also to incorporate indoor measurements in a REM in the framework of the resource allocation in hetnets according to the research activities done in WP1.3 (JRA 1.3.3.A).

Regarding the impact of channel model in the performance evaluation of wireless systems, the evaluation was comprehensive enough to validate the impact that different channel models (i.e., ITU Pedestrian B and 3GPP Extended Pedestrian A, at different speeds) have on the effectiveness of the evaluated interference-mitigation scheme and, ultimately, on the performance observed for the primary communication link. Nonetheless, a deeper evaluation is still required covering a more richer set of conditions (e.g., a single static custom channel was considered for the interfering signal). In this sense, the work will be extended to bring the operating conditions closer to the real-world (e.g., including the utilization of an indoor-to-outdoor channel for the interfering signal). This will allow to better characterize the impact of the considered channel model on the evaluation of the performance of a wireless communication scheme (i.e., a new measurement campaign will be performed using the channel models provided by JRA#C).

Regarding codes that achieve channel capacity, a first Belief Propagation (BP) decoding architecture has already been developed and synthesized to have a preliminary comparison with respect to alternative decoding approaches and codes. It can be noticed that, notwithstanding the different clock frequencies, BP decoder achieves a higher throughput than Successive Cancellation (SC): this confirms that BP decoding is a promising approach to target high throughput applications.

Regarding the assessment and development of multi-link channel models, a draft of the review paper has been circulated among partners and is under revision by the partners. The plan is to pursue and finalize this activity in the next period. Regarding the development of channel models, three activities are currently on-going: *i*) development of indoor multi-link channel models (UCL, UGgent): a first model was designed and the resulting submitted paper is now in revision. It is now being extended to include angular proprties, as well combined with room-electromagnetic theory to

include late components. This model also serves as a basis for interaction with JRA-H. A joint UCL-UGent experimental campaign was carried out in February 2014 to estimate the channel dynamics in various indoor environments. Measurement results are currently being analysed; *ii*) dense multipath depolarization modeling (UCL, UNIBO): the polarimetric properties of so-called Dense Multipath Components were investigated in various outdoor and indoor environments, relying on broadband measurements and Ray-Tracing simulations, and *iii*) extended ray-tracing modeling for UWB transmissions (UCL, FTW): an existing ray-tracing tool is being extended with UWB capability.

Finally, regarding indoor location, there is a working prototype consisting of a moving robot that houses a control board, inertial measurement devices, WiFi and Bluetooth interfaces. This platform is able to run data fusion algorithms for indoor location and provides repeatability in the experiments, hence allowing fair performance assessment. Next steps will consist of experimenting with different scenarios and configurations, including methods for rapid, low-cost on-site deployment.

4. ANNEX A1 - Technical Achievements

4.1 JRA#A - Enhanced NC-OFDM transmission with reduced spurious emission level

The detailed description of algorithms designed in connection with Track 1 is provided in Track 1 deliverables.

Here it will be described how testbed for measurement and modelling of Power Amplifier (PA) in USRP transmitter was build and what results has been obtained. Our approach is new as our PA is embedded into whole transmission chain of software radio. Typically, external amplifier was modelled by Vector Network Analyzer. The testbed build for USRP PA measurements at PUT lab is shown in Figure 4.1. The transmitted signal for USRP is generated on a laptop computer with GNU Radio software. In the balloon simplified scheme of USRP with WBX board is shown. The signal passes through nonlinear PA (AMP), switch and goes to TX antenna port. There are two switches Hittite Microwave HMC174MS8 used for switching between full-duplex and half-duplex modes. In our case, full-duplex mode is used, i.e. RX2 antenna connector is connected to RX path and TX signal path is connected to TX/RX antenna connector. The signal at the output of PA is attenuated by 2x26 dB = 52dB (by isolation of two switches) before being received in RX signal path. If the RX2 connector is terminated the non-perfect isolation of switches allows us to observe distortion caused by TX PA on the same laptop with GNU Radio installed. However, the signal will be distorted by imperfections of the RX path of the USRP device.

On the other hand it was possible to make more accurate measurements using high-end equipment available at PUT lab, i.e. Rohde&Schwarz FSL Spectrum Analyzer (SA) in IQ trace setup. MATLAB with Instrument Control Toolbox installed on another laptop was used to store the received IQ data.

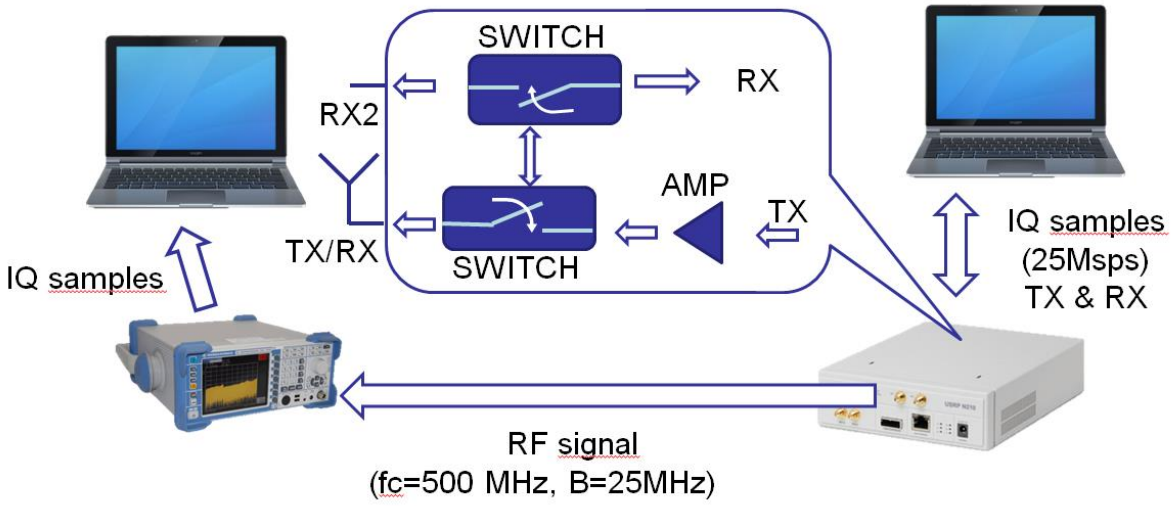

Figure 4.1 Scheme of the testbed for USRP TX nonlinearities measurements.

In order to obtain estimate of the distortion introduced by the measured amplifier a number of parameters has to be taken into account:

- Sampling frequency in the transmitter and receiver: At least the receivers should have bandwidth/sampling frequency a few times higher than the bandwidth of the transmitted signal. It is needed in order to observe third, fifth etc. order distortions. Moreover, only for transmitted signals of wide bandwidth memory effects of PA can be observed.

- Carrier frequency: The behavior of RF parts of the test setup may vary depending on carrier frequency. It can be the most visible in wideband devices as WBX board (50-2200MHz).
- Distribution of input signal amplitude/maximum amplitude of the input signal: It was shown previously that the distribution of input signal amplitude has influence on the estimated PA characteristic. The distribution of the signal used for PA characterization should be similar to the distribution of the signal used in normal runtime. Moreover, if signal amplitude exceeds 1 (in digital domain) in USRP device clipping in FPGA and DAC can be observed.
- TX/RX gains in USRP device and reference level of SA: It is important to use USRP TX PA efficiently, i.e. we use maximum TX gain. On the other hand it is important to set RX gain so that distortion caused by RX path in USRP device does not "hide" the nonlinear effects caused by TX PA. Similarly, SA has to be set as sensitive as possible but not to observe "overload" effects.

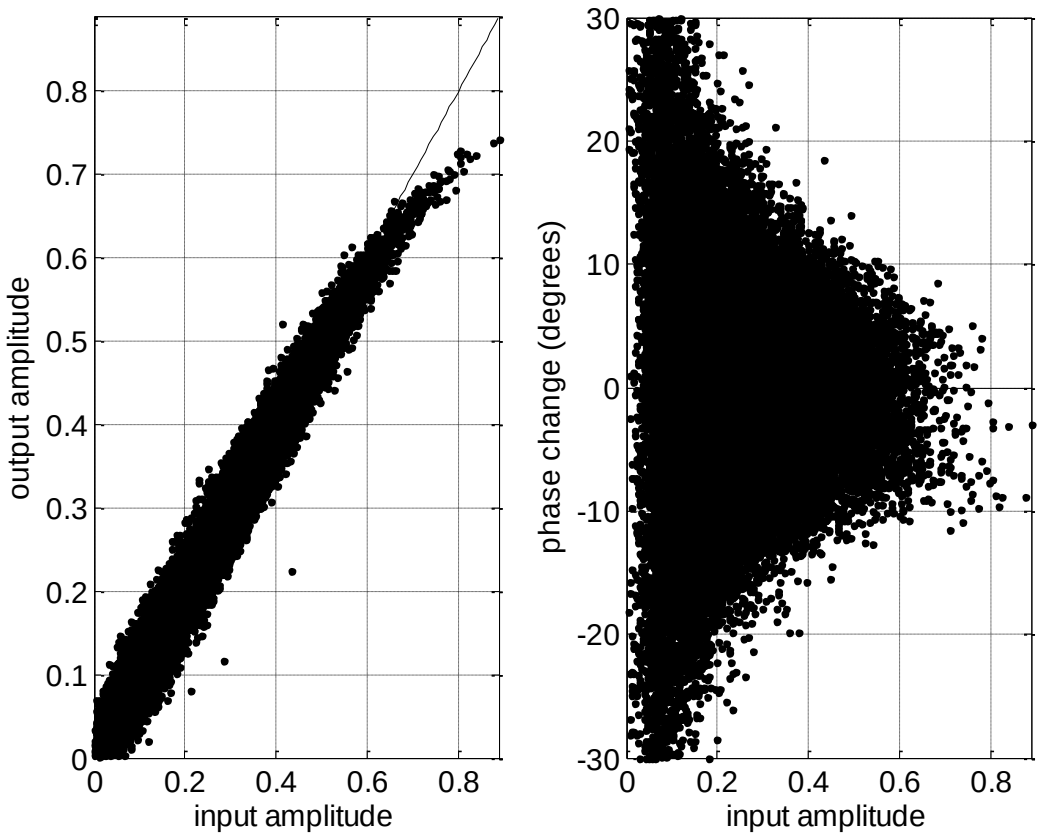

Figure 4.1.2 Characteristic of USRP+WBX PA obtained with SA with coarse time synchronization, no Carrier Frequency Offset (CFO) correction

It was chosen to transmit at carrier frequency 500 MHz, with sampling frequency 25 MHz in USRP device (both RX and TX) and 31.25 MHz in SA (that is further downsampled to 25 Msps). The maximum input signal amplitude was set to 0.888 and the signal consists of 10 random OFDM symbols generated with IFFT of size 4096 subcarriers. Not all subcarriers are used but only those lying around carrier frequency with occupied bandwidth of 5.62 MHz. The maximum TX gain was set, i.e. 25 dB, and it was observed 25 dB of RX gain provides best results (higher gain causes

intermodulation in USRP RX chain). For this setup signal received via USRP and SA was saved to file for post processing.

The received signal has to be aligned in time and in frequency with the transmitted one. First, coarse time synchronization is obtained by finding a peak in cross-correlation result. The resultant AM-AM and AM-PM characteristic (obtained with SA) is found in Figure . In case of ideal amplifier, both characteristic should be linear. In case of AM-AM characteristic saturation is observable. However, in both AM-AM and AM-PM characteristics variations of output for the same input amplitude is observed. It might be an effect of imperfect synchronization as well as a memory effect of PA. As both devices use different clocks, carrier frequency offset (CFO) can be estimated and reversed. By looking for the highest cross-correlation peak for different CFO values, the CFO of about 22.4Hz was found and reversed. In the resultant characteristic in Figure 4.1.2 it is visible that the AM-PM characteristic was improved, i.e. variation of phase change for a given input amplitude decreased.

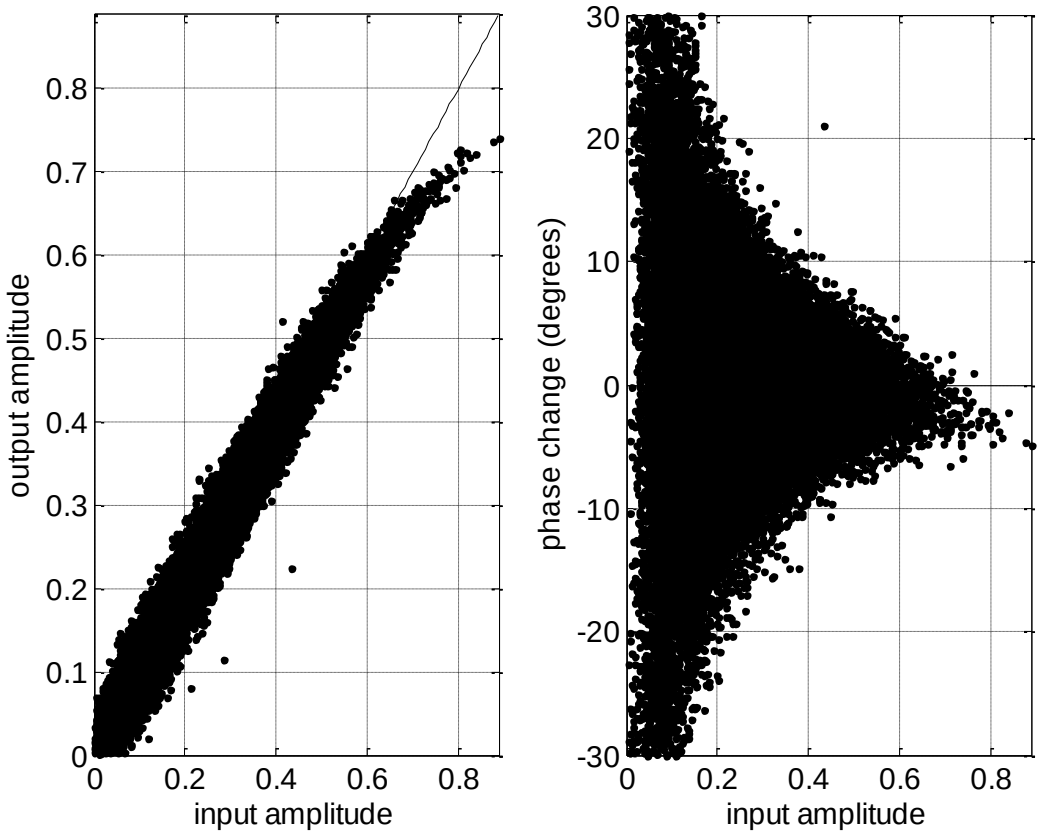

Figure 4.1.2 Characteristic of USRP+WBX PA obtained with SA with coarse time synchronization and Carrier Frequency Offset (CFO) correction

Although carrier frequency in both devices is now aligned and the sampling frequency is the same, time shift between sampling time in both devices can be observed. In order to obtain accurate time synchronization interpolation with Lagrange polynomial was used. For the first received test frame it was observed that time shift of 11.3ns was needed (while sampling period is 40ns). The resultant characteristics are shown in Figure 4.1.3. It is visible that variation of the output for a given input amplitude was significantly reduced. In order to reduce white noise influence that arises in all reception chains averaging over 100 consecutive frames can be conducted. The result after all explained processing stages is shown in Figure 4.1.4.

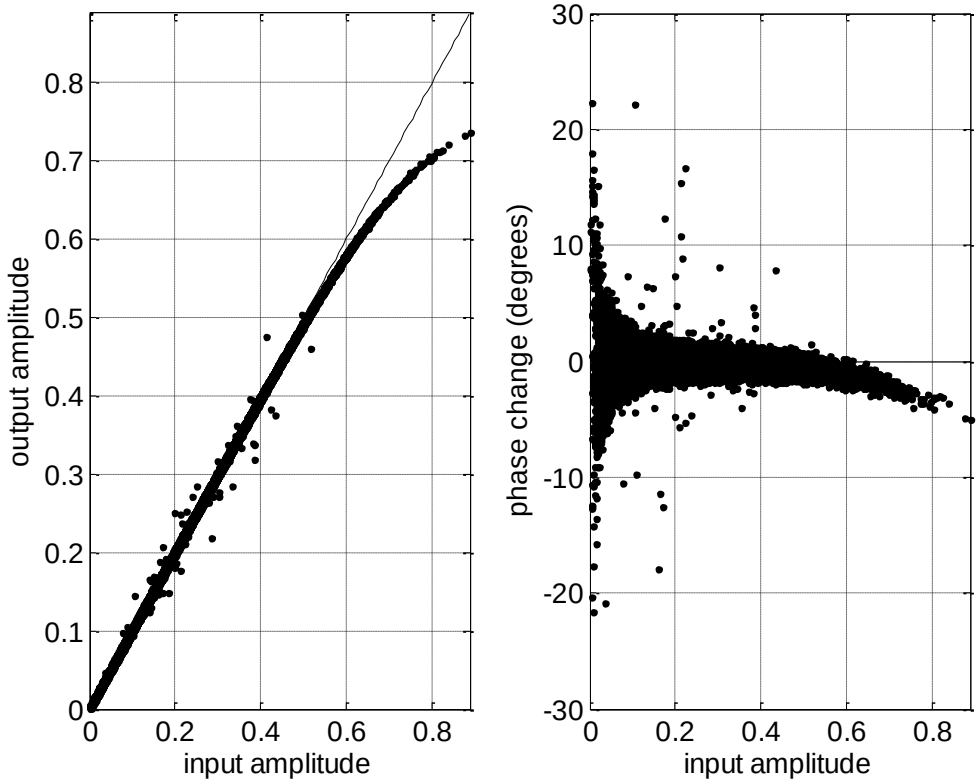

Figure 4.1.3 Characteristic of USRP+WBX PA obtained with SA with accurate time synchronization and Carrier Frequency Offset (CFO) correction

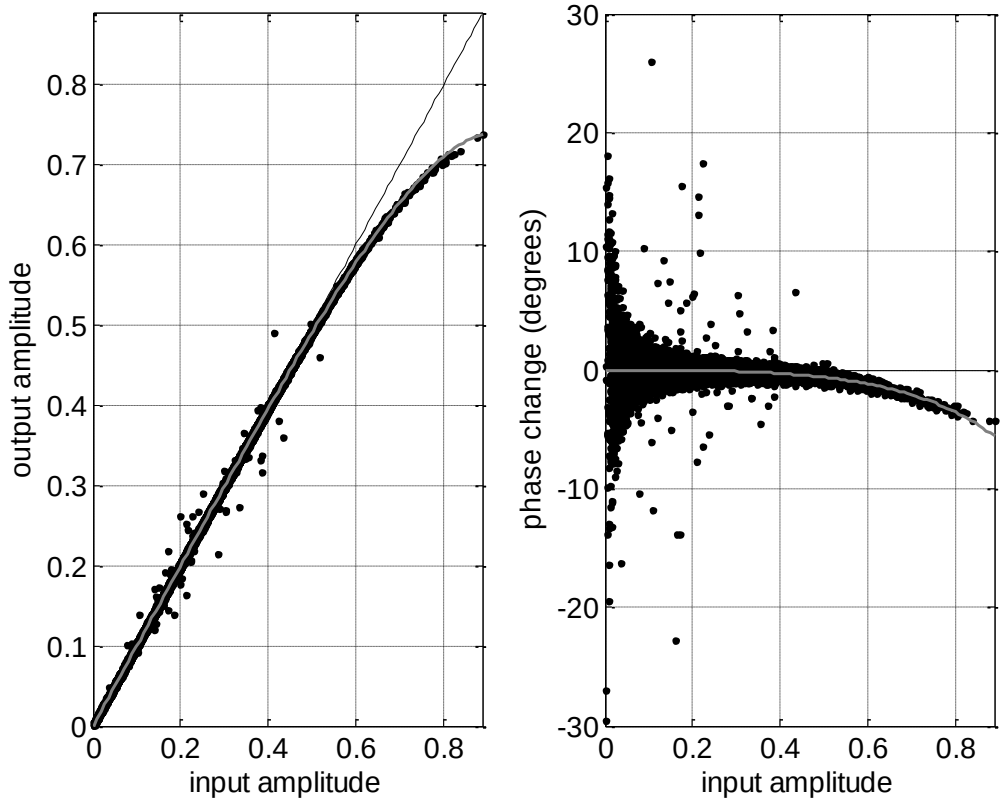

Figure 4.1.4 Characteristic of USRP+WBX PA obtained with SA with accurate time synchronization and Carrier Frequency Offset (CFO) correction, averaged over 100 frames

Based on the input samples and the corrected output samples parameters of memoryless polynomial model were estimated using least squares approximation. For x being an input sample the output of PA is y,that is modeled as:

$$y = x + (-0.0068 - i0.0134)x|x|^2 + (-0.2684 - i0.1138)x|x|^4.$$

Importantly, the coefficient of linear amplification above is set to 1, as previously normalization was carried. All PA coefficients were divided by the first one. Similarly, received signal was divided. As the reference signal is transmitted in digital domain, because of SDR usage, it would be hard to use absolute power values, e.g. dBm.

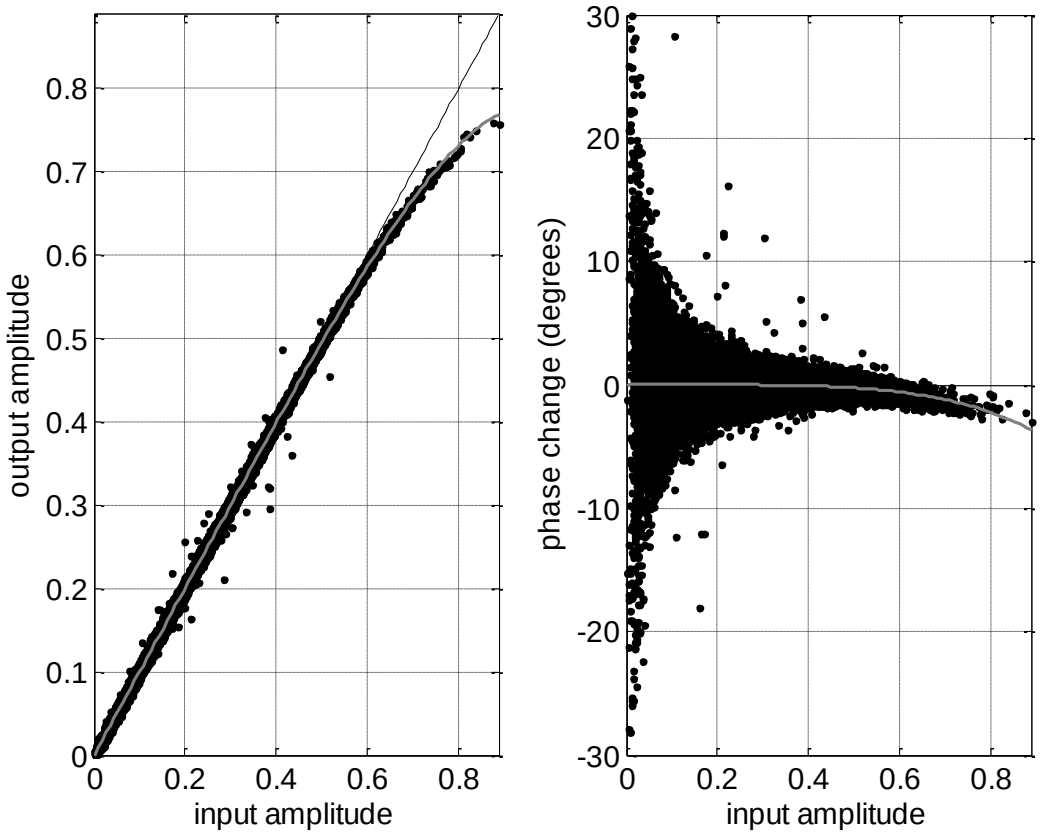

Figure 4.1.5 Characteristic of USRP+WBX PA obtained with USRP with accurate time synchronization and Carrier Frequency Offset (CFO) correction, averaged over 100 frames

We can compare this result with the PA model made with USRP RX side. The only difference is CFO estimation, that is not needed as USRP uses the same clock for both TX and RX side. The result is visible in Figure 4.1.5. The memoryless model obtained in this case is

$$y = x + (0.0614 + i0.0237)x|x|^2 + (-0.1827 - i0.064)x|x|^4$$

Although polynomial coefficients are different than in the previous case, both representations should give similar result. It can be justified by similar plots in Figure 4.1.4 and Figure 4.1.5.

4.2 JRA#B - Practical implementation of polar codes

Polar codes (PC) were recently introduced by E. Arikan [1]. Given their ability to (provably) achieve the capacity of symmetric binary discrete memoryless channels with low complexity encoders and decoders, they attracted wide interest from the communications community in exploring their theoretical limits, and recently in demonstrating practical implementations.

The central theoretical idea behind polar codes is the concept of “channel polarization.” That is, the encoder of a polar code repeatedly and recursively applies a linear transformation of N (the blocklength) desired bits, and sends this over the noisy binary (though one may generalize to larger alphabets) symmetric channel denoted by W. At the receiver, in Arikan's initial decoding scheme, the decoder successively decodes the bits. As a result of the repeated, carefully selected linear transformation, it may be shown that as the blocklength N grows, the new “effective channel” between the some of the initial bits and the outputs approach clean, noiseless channels, while the effective channels of other bits approach useless channels of zero capacity. Thus, the equivalent sub-channels are “polarized” to either be (nearly) completely clean or (nearly) completely noisy and useless. The fraction of clean channels approaches the capacity of W. The idea is then to fix the inputs to the useless channels and reliably transmit uncoded bits over the remaining clean channels. Arikan showed that there exist encoders and decoders of complexity $O(N \log N)$ that achieve the capacity of the channel W .

While the encoders of a polar code involve a relatively simple linear transformation, Tthe decoder is generally more involved and is central to any practical realization. Two types of decoders have been suggested: Arikan first proposed a successive cancellation (SC) decoder [1] in which the non-fixed bits are decoded in a particular order, and previously decoded bits are used in the decoding of subsequent bits. The second type of decoder proposed is based on belief propagation (BP) [2], which is an efficient way for solving inference problems based on passing local messages over bi-partite graphs consist-ing of “check nodes” and “variable nodes”. BP approximately computes the “beliefs” or conditional probabilities of the bits to be decoded given the channel outputs. It has been shown that under SC decoding, the decoding error probability of a polar code decays exponentially with the square root of the blocklength N (for large enough N). However, for moderate blocklengths N the performance of polar codes under SC decoding may be improved through the usage of the more computationally complex BP decoders. In fact, SC decoding may be seen as a specific instance of a BP decoder with a particular message passing or belief update schedule. Thus, at finite (and realistic) blocklengths N, one may thus intuitively trade-off performance for computational complexity.

In terms of decoder implementations in hardware, only a few solutions have so far been shown in the open literature. Most of them address architectures for FPGA and VLSI implementations of the SC decoding algorithm: computational resources are efficiently organized and scheduled in [3], [4] to achieve a very low implementation complexity; pipelining and look-ahead techniques are exploited in [5] to reduce the decoding latency by 50% and double the throughput. Given its larger computational complexity, the BP decoding technique has not received much attention thus far. An FPGA implementation of a BP-based decoder for PCs was proposed in [6], [7], but to the best of our knowledge, this is the first work that treats the VLSI design of a BP decoder for PCs. This short

work aims at showing that: (i) the BP algorithm applied to the decoding of PCs can be mapped onto a regular and efficient hardware architecture, (ii) the obtained implementation offers excellent performance in terms of both error correcting capabilities and throughput, at the cost of an occupied area four times larger than the best known SC-based decoder.

4.2.1 DECODING ALGORITHMS

Both SC and BP algorithms are based on the sparse factor graph representation of PCs [2], [8]. In SC decoding, the estimates of the transmitted bits are successively obtained from the received channel log-likelihood ratios y_i; the decoding of later bits exploits the already decoded bit values. In BP decoding, rather than making hard decisions, reliabilities (conditional probabilities) associated with different bits are propagated along the graph, in both forward (FW) and backward (BW) directions. A factor graph for code-length N = 8 is shown in Fig. 4.2.1, where N received y_i are indicated on the right side, the estimated transmitted bits u_i are on the left side and $\log_2$ N stages connect y_i and u_i, according to the code structure. After the initialization step in which nodes on the right are loaded with the received y_i, FW and BW runs are iterated a number of times.

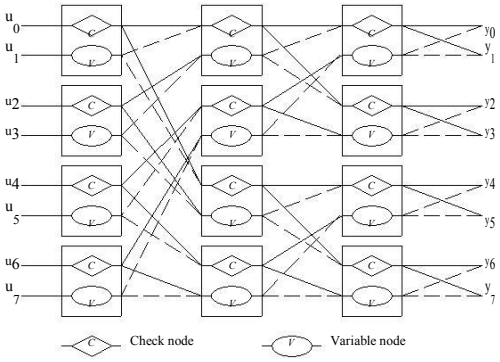

Fig. 4.2.1. Factor Graph of a Polar Code of length N = 8

The FW run proceeds along the $\log_2$ N stages of the graph. Each element includes a check (CN) and a variable node (VN). In the CN, the min–sum approximation is used for the $\boxplus$ operator, $x_1 \boxplus x_2 = \min\{|x_1|, |x_2|\} \cdot \text{sign}\{x_1 \cdot x_2\}$, while the VN evaluates $x_1 + x_2$. At iteration k, each graph element computes two output messages,

$$L_{o1}^{(k)} = L_{i1}^{(k)} \boxplus \left(L_{i2}^{(k)} + R_{i2}^{(k-1)}\right) \quad (1)$$

$$L_{o2}^{(k)} = \left(L_{i1}^{(k)} \boxplus R_{i1}^{(k-1)}\right) + L_{i2}^{(k)} \quad (2)$$

where inputs $L_{i1}^{(k)}$ and $L_{i2}^{(k)}$ are received from the previous stage while outputs $L_{o1}^{(k)}$ and $L_{o2}^{(k)}$ are propagated to the following stage in the factor graph. $R_{i1}^{(k-1)}$ and $R_{i2}^{(k-1)}$ are the messages evaluated at the same node during the previous backward iteration k − 1. In the BW run, messages are calculated in the opposite direction:

$$R_{o1}^{(k)} = R_{i1}^{(k)} \boxplus \left(R_{i2}^{(k)} + L_{i2}^{(k-1)}\right) \quad (3)$$

$$R_{o2}^{(k)} = \left(R_{i1}^{(k)} \boxplus L_{i1}^{(k-1)}\right) + R_{i2}^{(k)} \quad (4)$$

where $L_{i1}^{(k-1)}$ and $L_{i2}^{(k-1)}$ are the messages from the previous FW run. The final iteration consists of a single FW step, where hard decisions are finally made.

The higher computational complexity of BP (over SC) is due to the iterative nature of BP decoding; with this higher complexity comes better performance in terms of bit-error rates (BER) for finite code-lengths. As an example, the BER obtained when running the two decoding algorithms for N = 512 and N = 1024 cases are compared in Fig. 2. From the picture, it can be seen that, in the case N = 1024, BP outperforms SC by more than 1 dB at BER 10^{-5}.

One important point in the decoder implementation is the quantization of messages to a finite number of bits. As (1) to (4) include additions, the dynamic range of the messages tends to increase with iterations. However, a relevant fraction of the messages maintain values close to zero along the whole decoding process. As an example, message distributions for an N = 1024 polar code and signal to noise ratio (SNR) equal to 2.5 dB are shown in Figures 4.2.3 and 4.2.4. In particular, Fig. 4.2.3 provides distributions of right messages, taken at each iteration after the last forward step. Similarly, Fig. 4.2.4 reports distribution of left messages after the last backward step. Floating point arithmetic is used in these simulations. It can be seen that, in a finite precision implementation of the decoding algorithm, both accuracy in the representation of small values and dynamic range to represent large values are required. However, at this SNR level, most messages may be represented by a limited number of bits. Therefore, we adopt a fixed point representation with 8 or 9 bits and introduce saturation on values calculated by (1) to (4): in the 8 bits case, when an addition result is higher than 127 or lower than −128, it is set to 127 or −128 respectively. Curves in Fig. 4.2.2 show that the adopted quantization of left and right messages introduces an error floor below 10^{-6} and a small performance drop in the waterfall region.

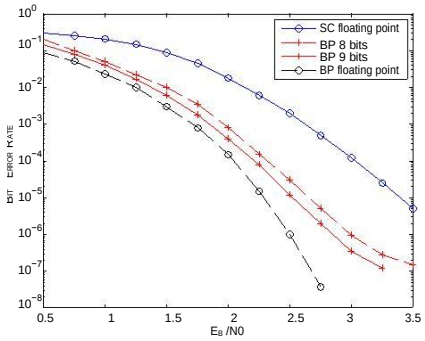

Fig. 4.2.2. BER performance comparison among unquantized SC, unquantized BP, and quantized BP decoding (8 and 9 bits).

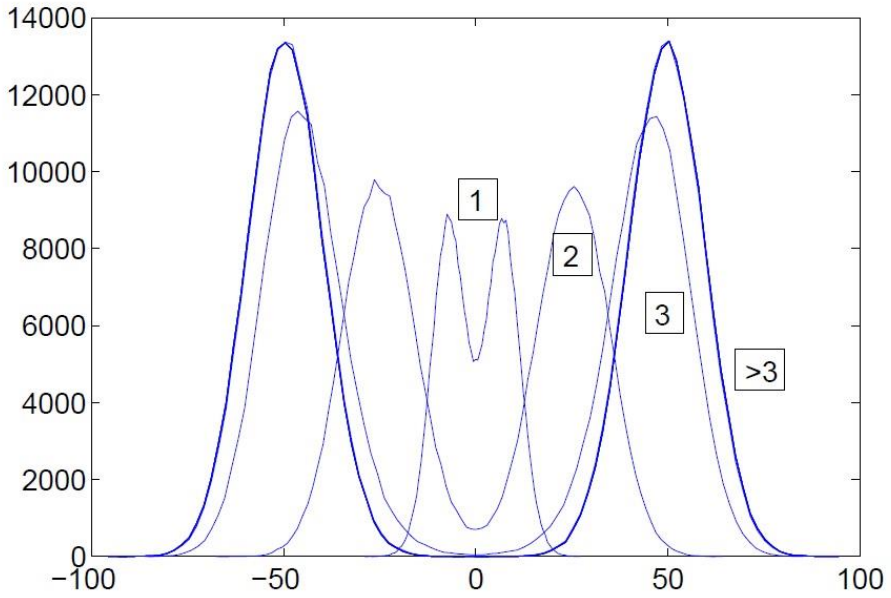

Fig. 4.2.3. Density function for right messages after iterations 1 to 10

4.2.2 DECODER ARCHITECTURE

BP decoding for PCs may be implemented using a serial processing architecture, with a single CN-VN pair sequentially running (1) to (4) on each node of the graph. With I iterations, rate r and clock frequency f_{CK} , the through-put achievable with such a serial architecture is given by $TP_{serial} = (r \times f_{CK}) / (I \times \log_2 N)$, which is too low for most practical applications.

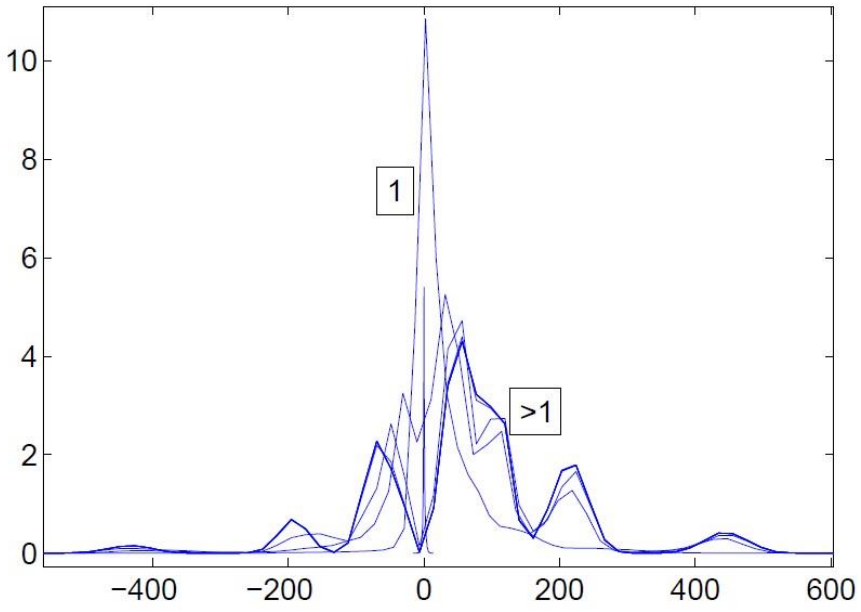

Fig. 4.2.4. Density function for right messages after iterations 1 to 10

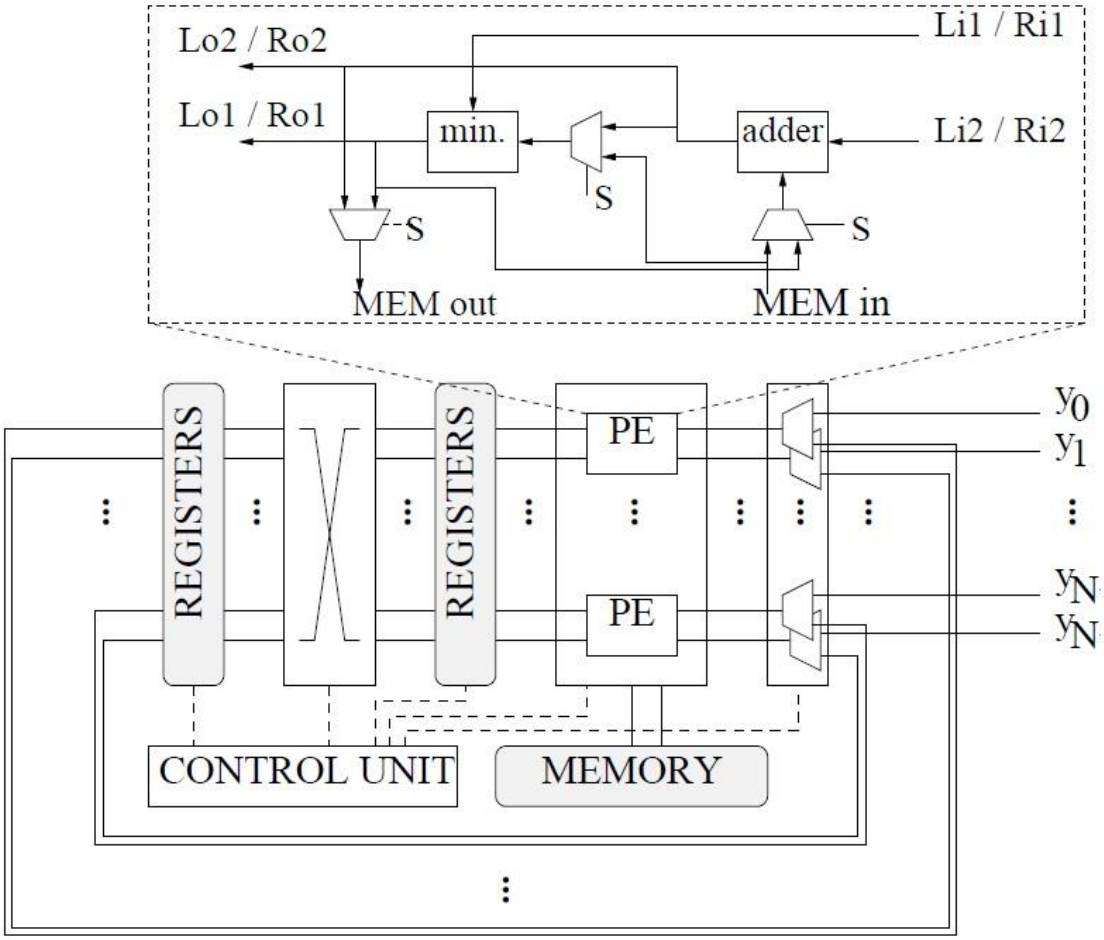

Fig. 4.2.5. Proposed PC decoder; components explained in *Decoder Architecture*.

For example, with N = 1024, r = 0.5, I = 10 and f_{CK} = 200 MHz, a throughput of 1 Mb/s is obtained. Higher processing speed may be guaranteed by using a fully parallel decoder, where a dedicated processing element (PE) consisting of a CN-VN pair is allocated for each node of the graph. In this approach, all nodes of a given graph stage could be executed concurrently in both FW and BW runs. However data dependencies between one stage and the following one do not permit full parallelism, resulting in poor hardware efficiency. In order to achieve a better hardware efficiency, a partially parallel architecture must be conceived: we propose to have $\frac{N}{2}$ PEs allocated to serve all nodes of a stage in parallel. A diagram of the proposed partially parallel decoder is given in Fig.5. The $\frac{N}{2}$ PEs concurrently execute

(1) to (4) on the nodes of a stage; the same units are reused to sequentially serve all graph stages. Eight bits have been selected to represent messages. Two sets of N registers are allocated to store input and output messages during both FW and BW runs. An additional memory stores messages related to the previous run: according to (1) to (4), when performing the FW run k each PE needs $R_{i_1}^{(k-1)}$ and $R_{i_2}^{(k-1)}$ messages, which were generated at the same graph node during the BW run k − 1 (similarly, $L_{i_1}^{(k-1)}$ and $L_{i_2}^{(k-1)}$ are needed in the BW run). Overall, N $\log_2$ N memory locations are necessary. The memory is managed as a circular buffer, where new data computed during a run progressively replaces data related to the previous one. The shuffle network reorders messages according to the structure of the graph in both FW and BW runs. A modular and

scalable butterfly network has been selected, as it is characterized by a small diameter ($\log_2 N$) and a small number of switching elements. The control unit generates memory addresses and schedules the decoding steps. Fig. 5 also details the PE architecture. Two input ports provide the couples L_{i1} and L_{i2} for the FW run or R_{i1} and R_{i2} for the BW one. Output ports return either L_{o1} and L_{o2} or R_{o1} and R_{o2}; these values are stored in the appropriate registers. The PEs also exchange data with the memory: the input port receives a right or left message stored at the previous run, while the output port allows writing the generated output message into the memory, where it has to be stored until the following run. Two key processing components are allocated in the PE: the min search and sign computation component executes the CN function (⊞ operator), while the adder component maps the VN function. The control signal S makes a distinction between the computation of the first and second output message: when S= 0, the PE executes (1) in the FW run or (3) in the BW run; when S= 1, either (2) or (4) are executed.

The nodes of a stage are concurrently updated in three clock cycles: two cycles are used by the PEs to generate the output messages (one cycle for L_{o1} or R_{o1}, and a second for L_{o2} or R_{o2}); the third stage is exploited to reorder messages across the shuffle network. Since we have $\log_2 N$ stages and each iteration is split into a FW and a BW run, one complete iteration takes $6 \log_2 N$ cycles, resulting in a throughput of $TP_{parallel} = (N \times r \times f_{CK}) / (6 \times I \times \log_2 N)$. For exam-ple, with N = 1024, r = 0.5, I = 10, f_{CK} = 200 MHz, the throughput is 170 Mb/s.

The straightforward implementation of the min component is shown in Fig. 4.2.6(a): assuming that inputs A and B are represented using two's complement values, the −A and −B have to be calculated and absolute values obtained by means of multiplexers. The sign s of the difference between the two absolute values is used together with the two signs of A and B to drive the selection of a four way multiplexer. If s = 0, it means that |A| > |B| and output C is equal to either B or −B based on sign(A). If on the contrary s = 1, |A| < |B| and output C is equal to either A or −A based on sign(B). Two subtracters are required to calculate −A and −B from A and B. Thus the complexity of the overall PE, which also includes the adder associated to the VN function, may be estimated as equal to four adders/subtracters, plus multiplexers.

Alternatively, messages may be represented by a sign and modulus. In this case, the min component reduces to a single subtracter, which directly computes the sign of difference between the two moduli, a multiplexer to select the smallest and an xor gate to generate the sign of the output. However the VN becomes more complex (Fig. 4.2.6(b)). Let x be the xor of the two signs. If x = 0, the two inputs have the same sign and the modulus of the output is |A| + |B|. If signs are different (x = 1), both |A| − |B| and |B| − |A| are computed.

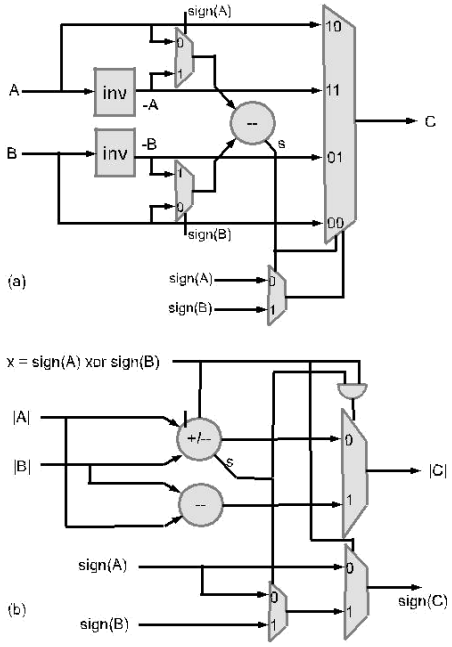

Fig. 4.2.6. Alternative implementation for the PE: (a) Min implementation with two's complement data, (b) Add implementation with sign and modulus data.

The choice between the two differences is made based on the sign s of |A| − |B|: if s = 0, |C| = |A| − |B|, otherwise |C| = |B|−|A|. The sign of the sum C is obtained separately: if x = 1 and s = 1, the sign of C is equal to the sign of B, otherwise it is set to the sign of A. Thus, the overall PE complexity with the sign and modulus representation is equal to three adders/subtracters (one for the min search and two for the addition), plus multiplexers and a few gates. From this high level estimation of the complexity, the sign and modulus representation are deemed to be less expensive in terms of the required resources.

The two PE schemes in Fig. 4.2.6 and the overall decoder architecture in Fig. 5 have been synthesized with the Synopsys Design Compiler, targeting a 90nm CMOS process and a clock frequency of 200 MHz. The two's complement PE data occupies an area of 1177 μm^2; the sign and modulus representation allows the reduction of the PE area to 649 μm^2 and therefore this second solution has been selected when implementing the whole decoder.

The main features of the proposed decoder architecture are reported in column 4 of Table I. An SC-based decoder is considered in column two [4], while column one reports implementation data for a fully parallel decoder optimized for a Low Density Parity Check (LDPC) code [9]. The occupied area of our decoder may be broken down as: RAM memories (70%), PE and registers (25 %), shuffle network (5 %). As for the SC-based decoder in [4], the occupied area is dominated by memories. The whole area could be reduced with a lower number of quantization bits, but this would introduce a larger performance drop with respect to the unquantized case. The Table also reports the achievable throughput, which is equal to 170 Mbps with 10 iterations. Notwithstanding the large difference in terms of clock frequency, this value is higher than the throughput shown in [4] for coding rate 1/2 and codeword length 1024. This difference in terms of speed between the two decoders in columns 3 and 4 is due to the greater level of parallelism incorporated in the BP-based decoder with respect to the SC one. The last row in Table I provides the required SNR to

achieve a BER level of 10^{-4} in the three considered decoders. It can be seen that the BP-based decoder attains coding gains of 0.4 dB and 0.8 dB over LDPC and SC-based decoders respectively.

TABLE I

COMPARISON AMONG POLAR AND LDPC CODE DECODERS

	[9]	[4]	This Work
Code	LDPC	Polar code	Polar code
Codelength	1024	1024	1024
Rate	1/2	1/2	1/2
N. of Iterations	64	-	10
Technology	160 nm	65 nm	90 nm
Quantization	4	6	8
Clock Frequency	64 MHz	500 MHz	200 MHz
Core Area	2.9 mm^2	0.35 mm^2	2.79 mm^2
Normalized Area @ 90 nm	0.92 mm^2	0.67 mm^2	2.79 mm^2
Throughput	1 Gb/s	123 Mb/s	170 Mb/s
SNR [@BER = 10^{-4}]	2.7 dB	3.1 dB	2.3 dB

4.2.3 References

[1] E. Arikan, “Channel polarization: A method for construct ing capacity-achieving codes for symmetric binary-input memoryless channels,” *IEEE Transactions on Information Theory,* vol. 55, no. 7, pp. 3051 –3073, july 2009.

[2] N. Hussami, R. Urbanke, and S. Korada, “Performance of pola r codes for channel and source coding,” in *Information Theory, 2009. ISIT 2009. IEEE International Symposium on*, 28 2009-july 3 2009, pp. 1488 –1492.

[3] C. Leroux, I. Tal, A. Vardy, and W. Gross, “Hardware archi tectures for successive cancellation decoding of polar codes,” in *Acoustics, Speech and Signal Processing (ICASSP), 2011 IEEE International Conference on*, may 2011, pp. 1665 –1668.

[4] C. Leroux, A. Raymond, G. Sarkis, and W. Gross, “A semi-para llel successive-cancellation decoder for polar codes,” *Signal Processing, IEEE Transactions on*, vol. PP, no. 99, p. 1, 2012.

[5] C. Zhang, B. Yuan, and K. K. Parhi, “Reduced-latency sc po lar decoder architectures,” in *Communications (ICC), 2012 IEEE International Con-ference on*, june 2012, pp. 3471 –3475.

[6] E. Arikan, “Polar codes: A pipelined implementation,” in *Proc. 4th Int. Symp. Broadband*

Communications, 2010 July 11-14 2010.

[7] A. Pamuk, “An fpga implementation architecture for decodin g of polar codes,” in *Wireless Communication Systems (ISWCS), 2011 8th Interna-tional Symposium on*, nov. 2011, pp. 437 – 441.

[8] E. Arikan, “A performance comparison of polar codes and ree d-muller codes,” *Communications Letters, IEEE*, vol. 12, no. 6, pp. 447 –449, june 2008.

[9] A. Blanksby and C. Howland, “A 690-mw 1-gb/s 1024-b, rate- 1/2 low-density parity-check code decoder,” *Solid-State Circuits, IEEE Journal of*, vol. 37, no. 3, pp. 404 –412, mar 2002.

4.3 JRA#F - Design and experimental validation of algorithms for active and passive indoor positioning

4.3.1 Introduction

Position aware systems are nowadays one of the most investigated topic and their importance is becoming wider and wider since hardware, software and services companies are doing relevant investments in indoor location and tracking technologies.

The knowledge of the position of a body inside a building allows to get several improvements in the way humans live and machines perform their jobs. There are many scenarios in which positioning systems can be exploited to get this improvement: they can be used to reduce the effort for elders and people with reduced mobility in reaching their destination, they can be integrated in robot to improve logistic platforms in big warehouses, they can be exploited by storekeepers in malls to guide their costumer to the shop. Many other applications can achieve better performances through indoor location.

Being able to estimate the position of a body (a person, a machine or an object) is a problem that has been investigated for many decades, in particular for the outdoor scenarios. In the last fifteen years the focus of researchers has moved also toward indoor. For the outdoor environment, there is one main technology enabling localisation: the Global Navigation Satellite System (GNSS). The GNSS operates exploiting constellation of satellites (i.e. GPS, GLONASS, Galileo and Beidou), orbiting around the Earth, that send to a ground receiver their position and the exact time. Collecting these informations from more than one satellite, the receiver is able to compute its position and time.

An Indoor Positioning System (IPS) is a system that continuously, real-time, automatically computes the position of an object in an indoor environment. It is worth to mention that in this context, the word "indoor" means a region of a building separated from the outside by walls. Because of this, indoor scenarios represent a challenge for GNSS systems typically. The satellite communication is not reliable inside the buildings because almost always the transmitter and the receiver are in non line-of-sight (NLOS) condition.

There are different ways to locate a body inside a building. Many of them rely on the interaction between some static devices, the anchors, and one or more moving devices. A map is required to known the environment characteristics. The anchors occupy a static and known position in the map. If the map is totally, or partially, missing the task of localise a body becomes part of a bigger problem called *Simultaneous Localisation and Mapping* (SLAM), which, as the name suggests, involves both the localisation of the body and the creation of the map describing the environment into which is moving.

It is possible to give the following definitions:

1. **Physical position** is an information on where a body is, expressed using coordinates (in a 2D reference system or eventually 3D). Moreover, depending on the chosen reference system,
   (a) **Absolute position** is expressed using a common reference system, shared among all the bodies in the area;
   (b) **Relative position** is expressed using another body (or a part of it) as reference system;

2. **Symbolic location** is an abstract information about the place occupied by a body, expressed in common language, in particular exploiting proximity idea.

4.3.2 Measurement techniques

1. Range and angle measurements, typically referred to multilateration or triangulation algorithm. The measurements provided by this technique are always related to the distance between an anchor (whose position is known) and the actual sensor on the moving device, which is able to identify the anchor that is sending the signal. There are several types of range measurements:

(a) **Time of arrival (TOA)** allows to compute the distance between the transmitter and the receiver: the time for the signal to reach the destination (time of flight tf) is proportional to distance d between the two devices, $tf \propto d$ (see figure 2.2(a)). TOA needs all the devices (transmitters and receivers) to be synchronised and, moreover, the timestamp must be transmitted to let the receiver know about the transmission instant;

(b) **Time difference of arrival (TDOA)** allows to compute the distance between one transmitter and several anchors considering the time difference inwhich the same signal reaches the anchors. This approach allows to relax the synchronisation constraints between the receivers and the transmitter;

(c) **Roundtrip time of flight (RTOF)** provides the measure of the distance between two transceivers A, B (see figure 2.2(b)), considering that the time needed for the signal to complete the roundtrip is proportional to double the distance between the two, that is
$t_{round} = t_{fAB} + t_r + t_{fBA}$
$t_r \ll t_{AB}, t_{BA} \longrightarrow t_r \simeq t_{fAB} + t_{fBA}$ (2.1)

where t_{round} is the roundtrip time, t_r is the response time of the target device and t_{AB}, t_{BA} are the time of flight from one device to the other and viceversa. Differently from TOA, it does not require

synchronisation between transmitter and receiver, but it could be affected by clock drifts, especially for large tr;

(d) **Received Signal Strength** is the measure of the received power at the antenna of the moving device. Fading is a critical issue for this kind of measurements. It can happen that power and distance are weakly correlated in particular scenarios. This kind of measurements will be discussed deeply in the following;

(e) **Phase of arrival (POA)** allows to compute the distance between a set of transmitter and a receiver measuring the difference in the phase of the received signal. POA requires synchronisation between all the transmitter and the broadcast of a pure sinusoidal tone. The drawback is the phase ambiguity if the range is greater than the wavelength of the tone;

(f) **Angle of arrival (AOA)** provides the measure of the distance exploiting one, or more, pairs of angle direction lines connecting the emitter and the receiver, expressed with respect to a known direction. AOA requires only two angles and two reference points (θ1, θ2 and A,B respectively in figure 2.2(c)) to determine the distance, actually the intersection between the angles' directions. The drawback of AOA is the hardware requirements: it needs very precise angles' measurements provided by directional antennas or antennas' arrays. Moreover AOA provides good results in short range distance, in fact the longer the distance between the anchors and the devices, the higher the error introduced in the position computation due to
the laws used to convert from angles to distance.

2. Scene analysis is based on the collection of point-wise measurements of the properties of one, or more, media, taken in the environment in which the system will run. The process of defining the points in which take measurements, and then measuring, is called site surveying. Typically, those measuring techniques are associated to the fingerprinting algorithm;

3. Proximity relies on a grid of sensing elements deployed in the environment. The measure itself is the presence or the absence of the target in the sensing range of the sensor connectivity.

4.3.3 Key performance indicators

There are several Key Performance Indicators (KPI) or figures of merit used to compare the features of different IPSs. The following are the most relevant and widely adopted.

1. **Accuracy** is the error committed in the position estimation, the Euclidean distance between the estimated position and the real position. Typically an average of the position error is taken into account, the mean distance error, as key performance metric. Standard deviation, minimum and maximum error values are other metrics of interest. Accuracy is often considered as the most relevant figure of merit;

2. **Precision** is the measure of the performance of the estimation over time or, from another viewpoint, how often the given accuracy can be achieved. As metric for precision the error standard deviation is adopted, which can be obtained computing the Root Mean Squared Error (RMSE) that is the sum of mean squared error plus the variance. This quantity can be gathered

from the knowledge of the error CDF. Moreover, in general, the faster the CDF graph reaches one, the better is the precision of the system;

3. **Robustness** is the capability of the system to work even if it runs out of the typical environment characteristics (i.e. number of anchors, type of anchors, availability of other target to share information with, etc.);

4. **Cost** is a KPI with several meanings, depending on the context and the system level taken into account. The system cost may include the deployment of the infrastructure (if is not already installed), the development of the algorithm (involving both measurements and programming), the hardware production and so on;

5. **Refresh rate** is the frequency at which new position estimation are computed. This periodicity is determined by several factors: the sampling frequency of the sensors, the computational power of the device, the complexity of the algorithm, etc;

6. **Complexity** is the description of how big is the computational effort to achieve the aimed performance (i.e. the combination of accuracy and other KPI). It can be referred to software computational load, hardware usage, database readings, etc.

Furthermore, there are some other relevant parameters that one should take into account while evaluating an IPS, such as the **commercial availability** of the required hardware/software combination; the **latency** (response time of the localization system, i.e., the required time for updating the location after a request for location estimation), the **energy efficiency** (especially important in wireless sensor networks), the **scalability** of the whole infrastructure to include new technologies, nodes and users; the **user preferences** among different technologies; and, last but not least, the **privacy** offered to the final user.

4.3.4 Technologies enabling indoor positioning

There are different technologies enabling indoor location (see [28, 42, 32, 30, ?] for a complete survey). Among them, the majority exploits wireless communication systems, in particular:

• **Bluetooth (IEEE 802.15.1)** is a technology used to create Wireless Personal Area Networks present in wide range of smart devices and portable computer. The measurements to locate the device are based on Received Signal Strength (RSS). The maximum range for this kind of network is 100m while the typical coverage (e.g. that provided by smartphones, tablets, laptops, etc.) is about 10m. The received power is affected by fading and this can reduce the accuracy in range estimation. In 2010, a new standard specification was published (Bluetooth Core Specification version 4.0 [16]), including the new Bluetooth Low energy protocol that allows very low-latency/low-power transmissions that could be exploited in the near future for very short positioning schemes or proximity sensing;

• **RFID** is a technology that allows to create passive tags that can be used to identify objects and goods (e.g. in stores, malls, warehouses, etc.). It can be used also to locate object. UHF (800-900MHz) passive RFID can range object at 6˜8 meters, inductive passive RFID have a range of some centimetres;

• **Ultra-Wide Band (UWB, IEEE 802.15.4a)** is a quite recent radio technology that makes use of large bandwidth signals (i.e. more than 500MHz). In the time domain, UWB signals are made of pulses having length in the order of hundreds of picoseconds. The replicas of the transmitted signal, generated by the reflections on the surfaces, can be filtered out because they do not overlap the original signal since their delay is appreciable (see figure 2.3). This capability reduces the interference and allows to determine the time-of-flight (TOF) of each single pulse with accuracy and then to compute the distance in a very precise way. Each anchor can cover a range of almost 400m2. This technology is very promising [18, 19] even if the penetration in consumer's market has not started yet;

• **WiFi (IEEE 802.11)** is one of the most diffused technologies to create Wireless Local Area Networks. Its market's penetration has reached very high percentage both in industrial and consumer markets today. WiFi access points are present in public places (e.g. squares, hospitals, malls, libraries, etc.), private houses and companies. The coverage inside buildings is of some tens of meters, depending on the selected transmission power and the type of walls and furniture. As for Bluetooth, the RSS is the measurements that can be exploited for localization purposes;

• **Wireless Sensors Networks (WSN)** are networks deployed for monitoring and actuation purposes [44], to control a specific area and/or to modify remotely the environment's properties. There are different standards that allow to create this kind of network. Among them the most diffused is the IEEE 802.15.4 that de fines the PHY and the MAC layers. On top of these, developers can use different layers depending on the deployment needs. Very common are ZigBee [11] and some other proprietary solutions. The location capability is provided by the RSS measurements.

Other technologies are available, not exploiting radio communication. Among those, the most relevant are:

• **Infrared** exploits the infrared light emission between a LED source (typically on the anchor) and a receiver, a phototransistor or a photoresistor, to determine the distance between the two. It requires line-of-sight between the two devices, no obstructions and no strong light impinging on the sensors. Because of these limitations, this technology has a range limited to the area defined by the nearest walls (i.e. a room);

• **Ultrasounds** that exploit sounds (i.e. air vibrations) having typical frequencies much higher with respect to those heard from the human ear. This technology allows to achieve good measurements accuracy, in the centimetre range. Ultrasounds can be used in two ways:

– **passive,** when there is only one ultrasound device capable of transmitting and receiving, that emits a sound and then hears the echo coming from the reflections with surfaces. These radar techniques are broadly used in SLAM problems and robotics;

– **active,** when there are some devices transmitting ultrasounds and the others receiving these signals. If the devices are synchronised (e.g. using RF signal to trigger the sound transmission) then it is possible to compute the distance from the fixed devices to the moving one.

• **Optical camera** exploits digital cameras to extract the environment's key features and then the position. It is a wide-spreading, expanding research field that has been speeded up, in the last years, thanks to the increasing computational capabilities of portable devices. In [34] four types of mutually non-exclusive optical IPSs are described:

– **Reference from 3D Building Models** that extract the informations about objects and bodies present in the environment and then compare these features with pre-recorded informations stored in a database;

– **Reference from Images** that is based on the comparison of sequence of images taken before, characterising an environment. This strategy is particularly challenging in terms of computational power since real-time motion analysis is required;

– **Reference from Deployed Coded Targets** that rests on physical image markers (typically 1D/2D barcode or specific coloured patterns), deployed along the building in known position, that allows the system to immediately recognise the position with low computational effort;

– **Reference from Projected Targets** that, similarly to Deployed Coded Targets, is based on pattern or particular shapes recognised by the system. In this case the markers are not deployed physically in the building but projected, eventually using non-visible light (e.g. infrared, laser, etc.).

• **Inertial Measurement Units (IMU)** could be added to this list, although they are not a positioning technology in a strict sense. IMUs does not provide directly a measure to estimate the position but instead an information about the accelerations and the rotations experienced by the device, which can be exploited in dead reckoning and data-fusion techniques, to improve the performances of the whole system.

Technology	Medium	Measurement	Pros	Cons
Bluetooth	RF	RSS	Availability, small size	Range, accuracy
RFID	RF	Proximity	Low cost, accuracy	Ultra short range
UWB	RF	TOF	High accuracy, large range	Availability, cost, size
WiFi	RF	RSS	Availability, good range	Accuracy
WSN	RF	RSS	Good range	Availability, custom solution
Infrared	Light	Intensity	Accuracy, size, cost	Range, light intensity dependent
Ultrasounds	Sound	TOF	Accuracy	Size, availability
Optical camera	Image	Image features	Availability, accuracy	Computational requirements

Table 1 - Technologies enabling indoor positioning

4.3.5 Testbed description

The mission of OpenInLocation Lab is to accelerate the development of cutting-edge indoor location solutions, featuring a mobile autonomous platform with the required hardware and software equipment to simulate indoor/outdoor real-life dynamic scenarios and allow for precise benchmarking trajectories and repeatability of experiments. The autonomous mobile robot (named after Gauss) consists of a mobile platform with motors, encoders, motor controller, IMU (with 3-axis accelerometer and gyroscopes), distance sensors and a navigation controller board with an Arduino Duemilanove microcontroller. This microcontroller controls the IMU, sensors, velocity and number of counts of the motors to perform the programmed trajectory. New trajectories can be programmed easily with straight paths and rotations. The position of the mobile robot during the trajectory is obtained through the number of counts of the motors and gyroscope measurements.

Autonomous mobile robot

The board has an Arduino Duemilanove compatible microcontroller with 6 ADC converters, 6 pins PWM output and UART/USB port. Four IR distance sensors are connected to four ADC converters.

The functionality of the code is showed in next diagram.

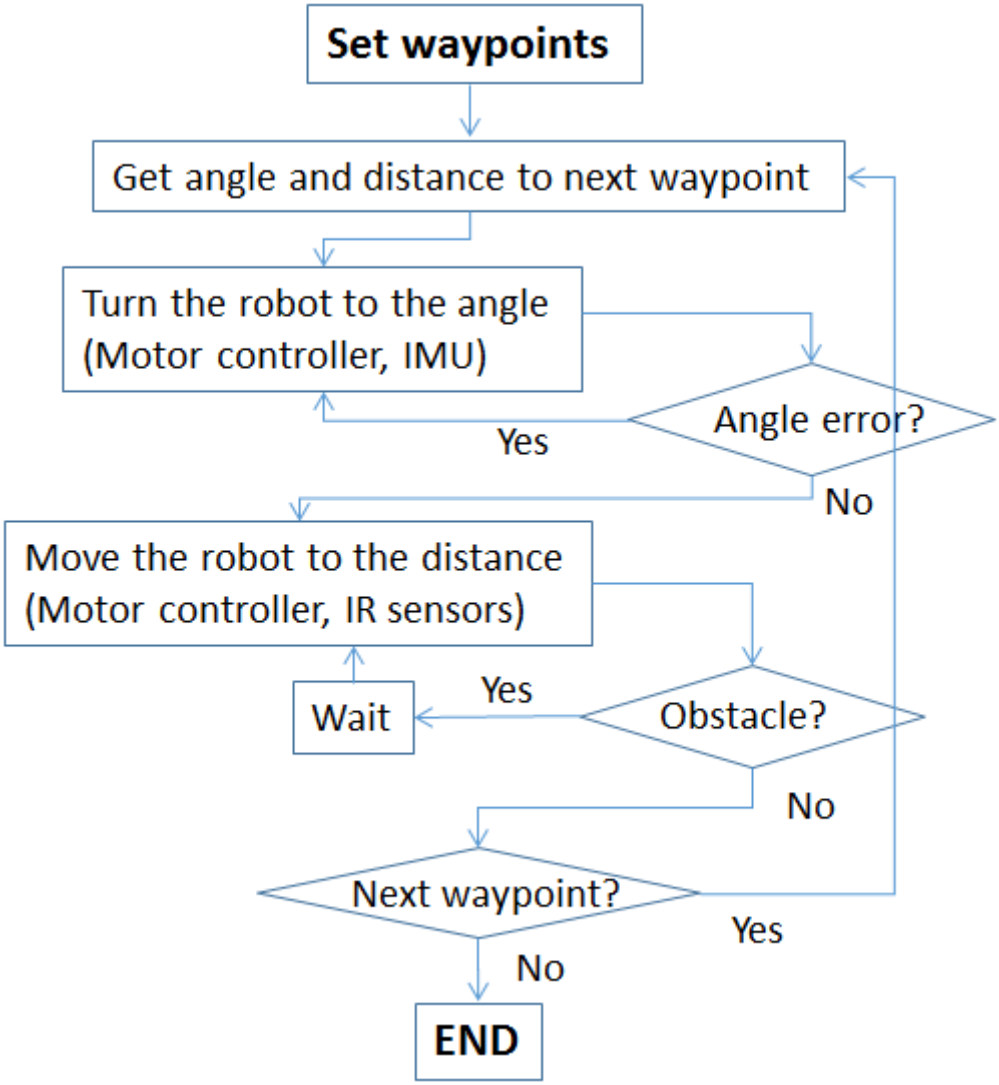

- Rotations with gyroscopes.
- Movement of the robot to next waypoint and avoiding of obstacles.
- Coordinates of the robot and position estimation from origin.
- All the information managed by the Raspberry Pi.

Positioning Payload for Indoor Positioning

The robotic plaform includes a positioning payload where indoor positioning and mapping algorithms could be easily implemented and tested with the platform.

The positioning payload (see Fig. 4.3.5.1) is a development board with multiple connections where positioning algorithms can be easily implemented. It consists of a RaspberryPI board model B, an IMU (3-axis gyroscope, 3-axis accelerometer, 3-axis magnetometer, digital barometer) and a USB WiFi card (IEEE 802.11n, 802.11g, 802.11b). The RaspberryPI board has a CPU ARM11 @700 MHz featuring floating point ALU with Ethernet, USB 2.0, I2C, serial port and GPIOs, Linux O.S (debian-based distribution) and dedicated HD camera connector.

The positioning payload is a cheap and easy-to-use system that allows WiFi RSS reading, IMU (inertial data) reading, Bluetooth 4.0/LE (small range location) with a CPU power (similar to an entry level smartphone).

The overall system consists of the positioning payload and the data base. The Raspberry Pi microcontroller sends the RSS and inertial measurements to the data base of the server. These data are used by the positioning, tracking and data fusion methods to estimate the coordinates of the mobile robot. In figure 4.3.1, schematic of the overall system is seen where the positioning payload reads RSS WiFi measurements and Inertial data. Data fusion algorithms can be implemented and tested in this platform or logged into a database for off-line processing purposes.

The OpenInLocation lab allows researchers to test and validate their algorithms (implemented in the positioning payload) in the Gauss robot (see Fig. 4.3.2). The mobile robot is used with the positioning payload to perform positioning in dynamic scenarios. It sends to the Raspberry Pi microcontroller its coordinates during the trajectory, which can be compared with the position estimate delivered by the algorithms to have an accurate benchmark of its accuracy. In the figure below, it can be observed the Gauss robot incorporating a WiFi dongle (elevated to emulate a smartphone carried by a human being), an IMU, and the positioning payload with a fusion algorithm.

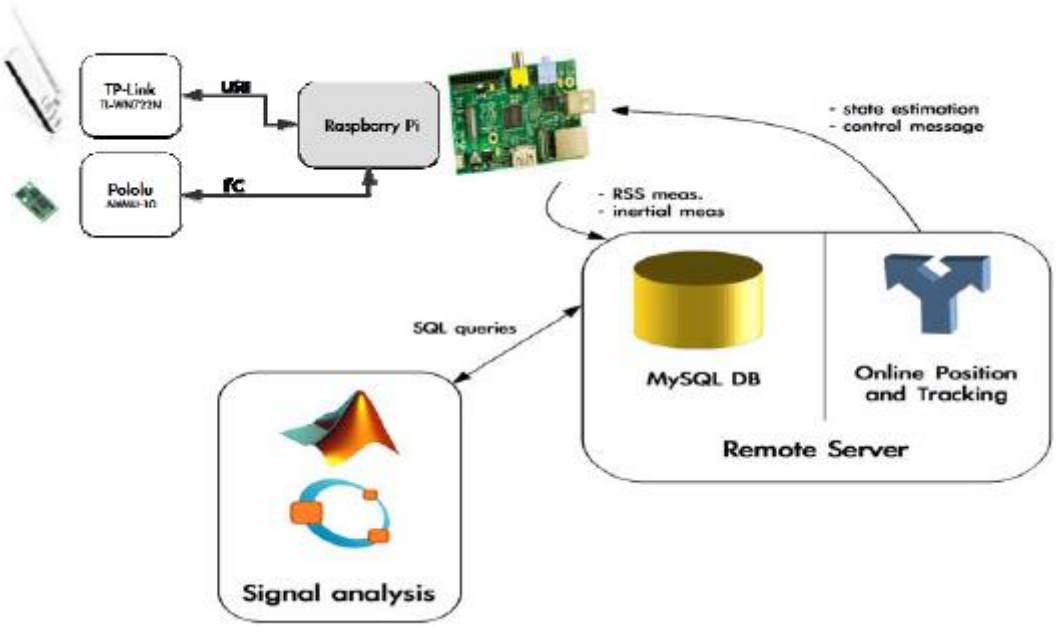

Figure 4.3.1. Schematic view of the positioning payload for a WiFi/IMU case.

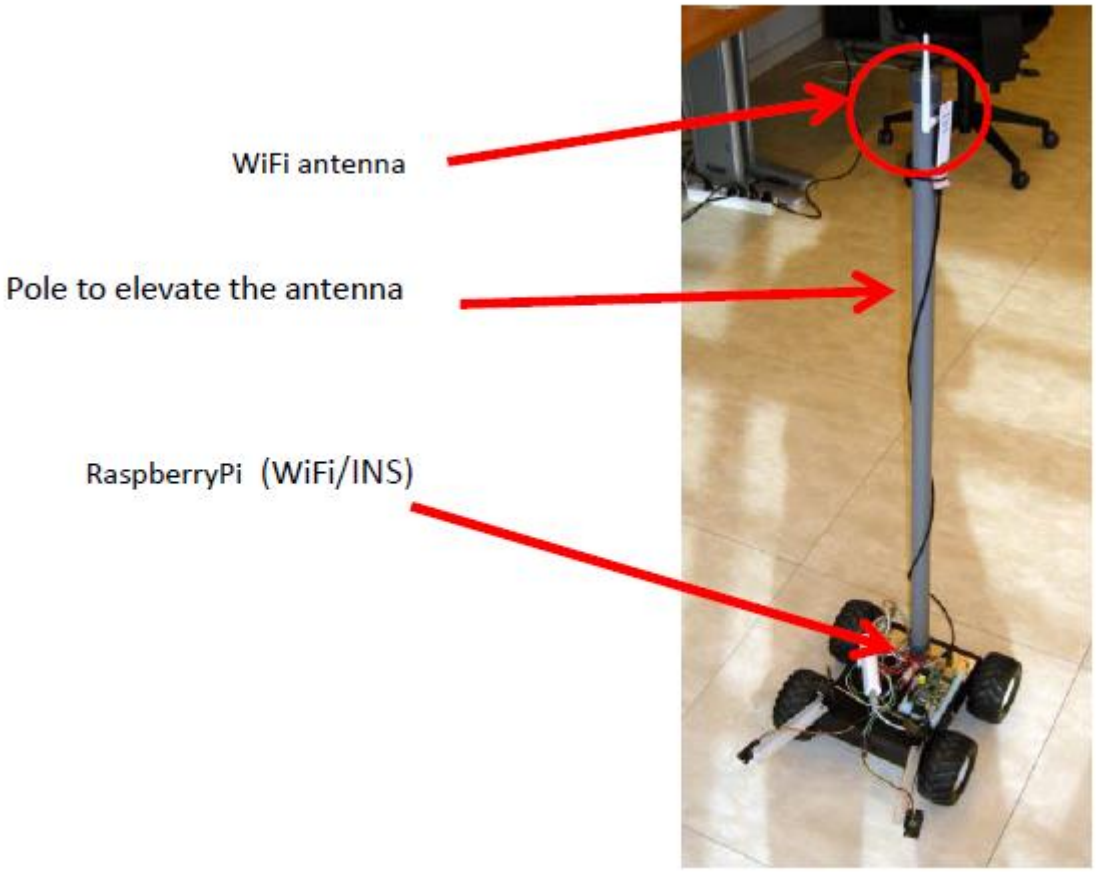

Figure. Picture of the overall test of a WiFI/IMU IPS algorithm mounted in the testing and validation Gauss platform.

4.4 JRA#G - Spectrum occupation measurements and database exploitation

4.4.1 TVWS Indoor Measurements for HetNets

This study focuses on analysing the potentials of TVWS for deploying small cells in indoor scenarios. This scenario is considered as particularly relevant for two main reasons. Firstly, most of broadband data traffic is generated indoors, so the deployment of small cells inside buildings (e.g. 3G and LTE femto-cells, APs, etc.) becomes a better solution to achieve high capacities than providing coverage from external cells. Secondly, it is expected that the availability of TVWS spectrum can be increased indoors thanks to the building penetration losses between indoor small cells and TV receiving antennas usually located at the rooftop. Due to the intrinsic randomness associated to propagation in indoor environments, the assessment of the capability of using TVWS needs to be done by means of exhaustive measurements. Then, we analyse this capability through an indoor measurement campaign made in two different locations of Europe, namely Barcelona and Poznan, exhibiting different occupation of the TV channels.

4.4.1.1 *Measurement set-up*

The measurement campaign has been carried out at two big European cities, namely Barcelona and Poznań, both of them with different existing allocations of DTV channels.

The location for the measurements in Poznań was the building of the Faculty of Electronics and Telecommunications of the Poznań University of Technology (PUT) (52 º 24' 1.58" N, 16º 57' 21.06" E). A total of 7 DTV channels were detected at the rooftop. Among them, detailed indoor measurements have been performed at channels 23 (490 MHz), 27 (522 MHz), 36 (594 MHz) and 39 (618 MHz). Channels 23, 27 and 39 come from a transmitter distanced by 31.5 km and transmitting at 100 kW power. Channel 36 is a SFN (Single Frequency Network) and comes from two transmitters distanced by 4.6 km and 19.2 km with transmit powers 10 kW and 5 kW, respectively.

The location for the measurements in Barcelona was the building of the Department of Signal Theory and Communications in the UPC Campus Nord (latitude: 41º 23' 20" N; longitude: 2º 6' 43" E; altitude: 175 m). A total of 21 DTV channels were detected at the rooftop. Among them, detailed indoor measurements have been performed at channels 26 (514 MHz), 44 (658 MHz) and 61 (794 MHz), located in the lower, middle and upper parts of the DTV spectrum, respectively. The three channels are received from a transmitter located at 3.1 km with transmit power of 10 kW for channel 26 and 7.4 kW for channels 44 and 61.

In both locations two types of measurements have been carried out, i.e. we have checked how the measured parameters changes in time and how they behave as a function of the location inside the building. In the first case dedicated measurement points have been identified (seven points in Poznan and four points in Barcelona, indicated as black dots in 0), while for the second case the measurements were done along the buildings' corridors (around 100m long in case of Poznan campus, and 30m long for Barcelona case).

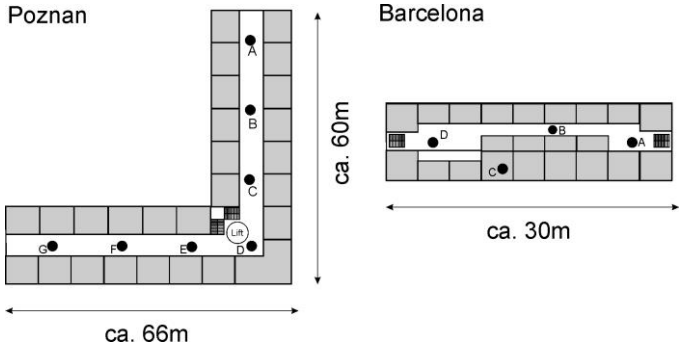

Fig. 4.4.1 Illustrative floor plans for both locations (Poznan and Barcelona) with indicated measurement points

In both cases the DTV signal was measured by the omnidirectional antenna, then sent to the spectrum analyzer and finally stored on the portable computer via Matlab. In case of Poznan measurements active quad antenna, covering 40-850MHz (1-69TV channel), was connected via coaxial cable Lexton 3C2V of length 3m to the R&S FLS6 spectrum analyzer. In Barcelona scenario the passive discone antenna of type AOR DN753 was used, covering the frequency range from 75 to 3000MHz, and connected to ANRITSU MS2721B device. The system setups are shown in 0 and 0. In both setups the resolution and video bandwidth of the spectrum analyzers were the same and equal to RBW=30kHz and VBW=100kHz, respectively.

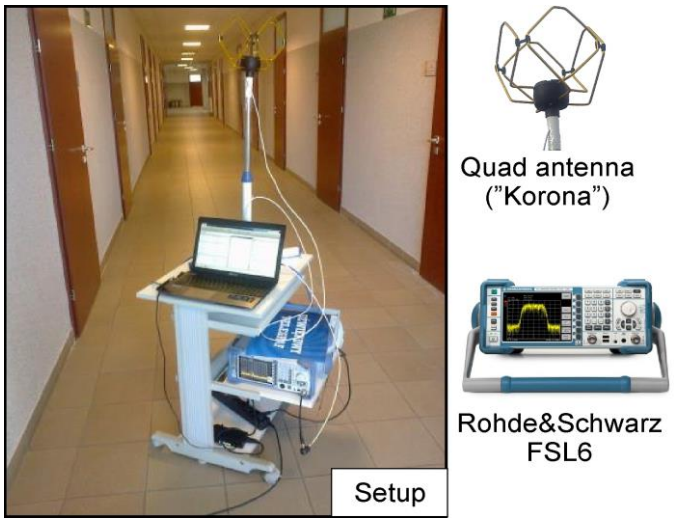

Fig. 4.4.2.Measurements system setup in Poznan

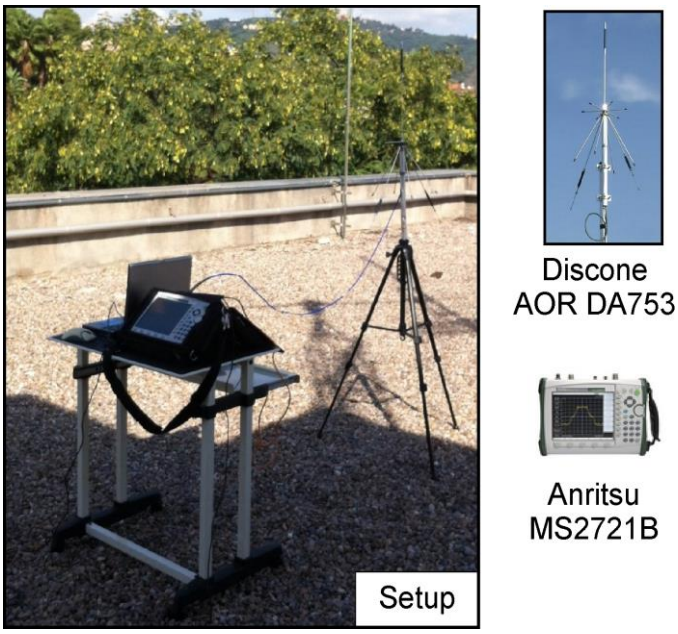

Fig. 4.4.3 Measurements system setup in Barcelona

4.4.1.2 *Measurement analysis*

The goal of the performed measurements was to analyze various parameters of the TV signals received inside the building for possible reuse of vacant TV channels for deployment of heterogeneous networks. In this section we present some of the measured features of the received signals that are important for future creation of digital REMs used for deployment of small-cells indoor transceivers. These are inter alia stability of the received signal over time, variations of the received power in terms of location, and influence of walls or people working/walking inside the building.

1) Average received power

As the first step the averaged power of the received TV signals in the selected points across the vertical profile of the building was measured (thus in each of the selected points the average received power within one 8-MHz width TV channel was measured on the roof, and on second, first and ground floor, and – only for Barcelona – in the underground). Some selected measured

values for different channels for Poznan and Barcelona are presented in the tables below. Moreover, the plot of the observed power spectral density in point D at rooftop and in the second floor is shown in 0. From that figure one can observe quite big differences between the roof and indoor measurements, i.e. besides high roof/walls attenuation various spikes of relatively high power have been detected indoor that come from various internal (i.e. deployed inside building) devices e.g. video cameras, computers, lightning etc. mounted near point D. Moreover, the amplification of the noise floor (which can be treated as ambient noise) observed in the frequency range 500- 700MHz is probably caused by some internally deployed devices.

Table 2 Average received power in Barcelona, Ch. 26

Channel 26	A	B	C	D
Rooftop	-44.41 dBm	-44.41 dBm	-44.41 dBm	-44.41 dBm
2nd floor	-62.06 dBm	-60.94 dBm	-63.13 dBm	-61.12 dBm
1st floor	-56.61 dBm	-57.06 dBm	-66.27 dBm	-55.96 dBm
Ground floor	-64.38 dBm	-57.67 dBm	-72.83 dBm	-63.00 dBm
Underground	-70.99 dBm	-68.71 dBm	-76.17 dBm	-74.40 dBm

Table 3 Average received power in Barcelona, Ch. 44

Channel 44	A	B	C	D
Rooftop	-46.76 dBm	-46.76 dBm	-46.76 dBm	-46.76 dBm
2nd floor	-60.77 dBm	-55.21 dBm	-60.52 dBm	-59.46 dBm
1st floor	-56.66 dBm	-51.89 dBm	-56.90 dBm	-63.62 dBm
Ground floor	-58.97 dBm	-52.29 dBm	-63.34 dBm	-59.73 dBm
Underground	-69.71 dBm	-67.08 dBm	-70.49 dBm	-69.56 dBm

Table 4 Average received power in Barcelona, Ch. 61

Channel 61	A	B	C	D
Rooftop	-58.12 dBm	-58.12 dBm	-58.12 dBm	-58.12 dBm
2nd floor	-68.88 dBm	-65.65 dBm	-70.98 dBm	-67.19 dBm
1st floor	-64.28 dBm	-60.45 dBm	-74.23 dBm	-68.24 dBm
Ground floor	-67.43 dBm	-64.04 dBm	-76.07 dBm	-63.61 dBm
Underground	-78.10 dBm	-76.85 dBm	-77.54 dBm	-77.77 dBm

Table 5 Average received power in Poznan, Ch. 23

Channel 23	A	B	C	D
Rooftop	-48.29 dBm	-49.78 dBm	-44.62 dBm	-46.68 dBm
2nd floor	-71.61 dBm	-68.68 dBm	-68.24 dBm	-64.09 dBm
1st floor	-73.25 dBm	-71.66 dBm	-79.14 dBm	-73.54 dBm
Ground floor	-80.31 dBm	-79.38 dBm	-81.37 dBm	-76.20 dBm
Channel 23	**E**	**F**	**G**	
Rooftop	-	-	-	
2nd floor	-63.75 dBm	-60.44 dBm	-63.94 dBm	
1st floor	-73.07 dBm	-71.17 dBm	-76.19 dBm	
Ground floor	-76.03 dBm	-77.2 dBm	-78.77 dBm	

Table 6 Average received power in Poznan, Ch. 27

Channel 27	A	B	C	D

Rooftop	-43.57 dBm	-45.15 dBm	-41.07 dBm	-42.99 dBm
2nd floor	-68.17 dBm	-66.22 dBm	-64.37 dBm	-62.63 dBm
1st floor	-72.28 dBm	-69.79 dBm	-71.85 dBm	-72.94 dBm
Ground floor	-77.30 dBm	-77.22 dBm	-75.96 dBm	-75.32 dBm
Channel 27	**E**	**F**	**G**	
Rooftop	-	-	-	
2nd floor	-65.98 dBm	-60.13 dBm	-64.94 dBm	
1st floor	-72.29 dBm	-68.56 dBm	-67.27 dBm	
Ground floor	-72.64 dBm	-75.75 dBm	-76.37 dBm	

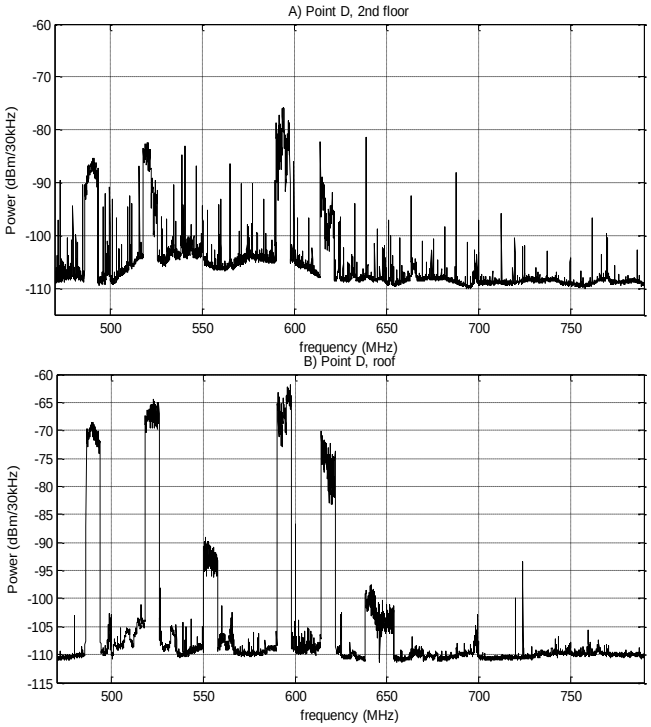

Fig 4.4.4 Power spectral density of the TV Band in Poznan at point D: a) at the second floor, b) at the rooftop

2) Stability over time

Although the average received power in different locations of the building is an important factor, it does not illustrate the real behaviour of the signal since the averaging process of the received power smoothes the temporal variations of this parameter. Therefore the stability of the received power over time has been selected as the second figure of merit that has to be verified. The measurements have been performed in different day phases and repeated for different days of the week and for different durations. In all cases the observed results were very similar to those presented below, i.e. although the received power varies in time, these variations are small enough to allow us state that there is high stability of the received power over time regardless of the daytime. Exemplary plots for both Barcelona and Poznan campuses are presented in 0, where the non-averaged received signal samples are collected over 30 minutes. The difference between the PUT and UPC results are due to the differences of spectrum analyzers performance, i.e. the sweep time for the same RBW and VBW over one TV channel was longer in a case of the device used in Barcelona. However such a feature does not influence the overall observation, that the variance of the measured power is very low. Let us stress that the value of the power variance was

always lower than 0.7dB, what allows us to state that for every TV channel there is a very little time variation of the received power.

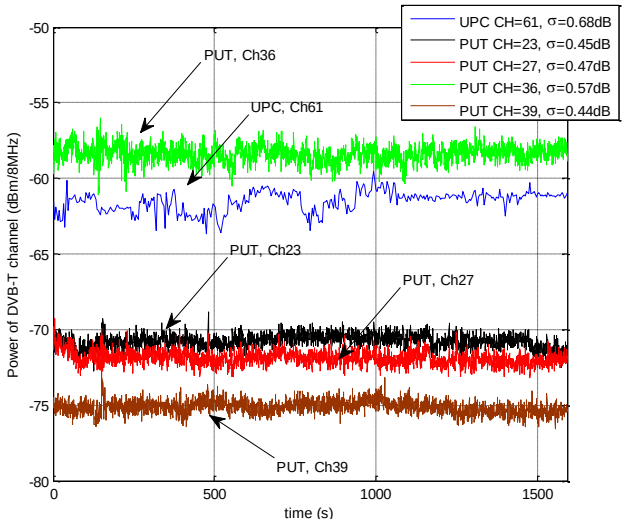

Fig. 4.4.5 Received power (non-averaged) observed over around 30 minutes

3) Crowded vs empty offices

0 shown above illustrates the changes of the received power as a function of time but in the situation where there were no or very few persons in the vicinity of the reception antenna. In order to be able to draw any reliable conclusions on the possible deployment of heterogeneous networks operating in TVWS, the radio environment maps have to take into account quotidian utilization of the premises (offices, class-rooms etc.). Therefore dedicated measurements have been performed in order to highlight the difference between crowded and empty offices. Analogous plot to 0 but for the crowded offices has been presented in 0.

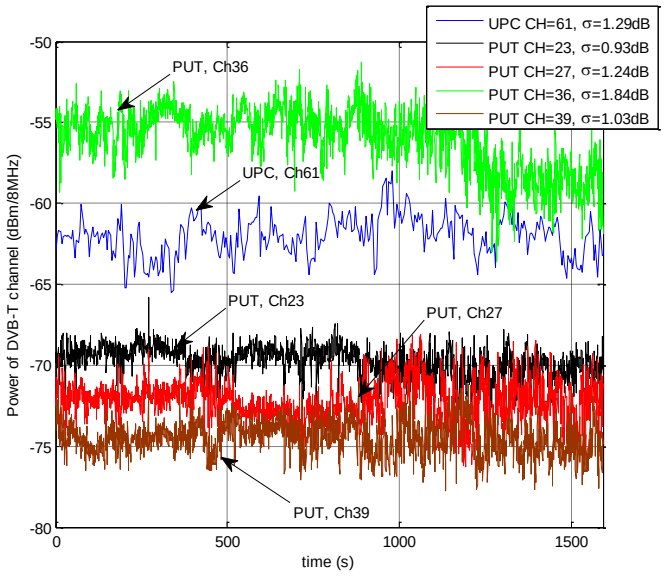

Fig. 4.4.6 Received power (non-averaged) observed over around 30 minutes – crowded premises

Comparison of these two figures brings us to the conclusion that the channel power is again quasi-stable in the sense, that the power variance has increased to maximally 1.8 dB. In general however, such an observation means that the quotidian usage of the premises does not impact on

the stability of the received power. Similar results have been observed regardless of the place of measurements, i.e. if the reception antenna was located on the corridor or inside the offices or class-rooms.

4) Dependency on location

In the process of REM creation for the heterogeneous networks the influence of Doppler and multipath effects cannot be omitted. Clearly, in the case of static receivers or mobile terminals used inside the building the effect of speed can be neglected. Contrarily the influence of multipath phenomenon will play a crucial role. Thus dedicated measurements have been performed aiming at finding the relation between the received signal power and the location inside the building. For that purpose walk-tests have been done, in which the averaged power in the TV band has been measured every 30 cm (in case of Poznan) and every 40 cm (in case of Barcelona) along the corridor. Such a plot is shown in 0. One can observe that in both locations the variance of the measured signal was around 4-5 dB. In each point the measurement was averaged over 10 sweeps that decreased strongly the variance of samples coming from time domain (0). Therefore, we can assume that all variations in received power are caused by the multipath effect connected with the location, and not with the time variations.

Furthermore, these measurements have been repeated in various days of the week in order to check the potential influence of quotidian usage of the building and surrounding area on the propagation conditions (0). The overall conclusion is that the behaviour of the signal inside the building in the same positions is stable over time. Let us stress that the smoother shapes of the curves in that plot compared to 0 are due to the applied averaging procedure. In other words, the moving averaging function over 10 samples has been applied in 0. For this reason, the value at the current location takes into account also the measurements from the neighbouring locations, i.e. 3 meters.

5) Influence of walls

Finally, some post-processing of the collected data has been performed in order to illustrate the average influence of each floor on the received signal (0). In other words, our goal was to measure the average attenuation (independent of the location and time, thus averaged over both location and time dimensions) observed at each building level. The attenuation shown in that figure is related to the power observed at the rooftop, thus one can conclude what is the influence of the given floor on the received signal strength.

Three main conclusions can be drawn: first, as expected, there is high relation between the received signal power and the location in the vertical profile of the building. Second, the solid green (with triangular markers) is much stronger than others and the reason for that situation is that this is the only one available SFN channel and the distance from the DVB-T transmitter is the smallest. Third, significant impact of the building construction is observed in the case of UPC, where the attenuation on the first floor is slightly lower than on the second floor (for each TV channel). In fact, in this case the transmitter is located at only 3.1 km from the building with almost line-of-sight conditions for all the floors (except the underground), meaning that the main attenuation comes from the wall penetration losses, which are similar for all the floors.

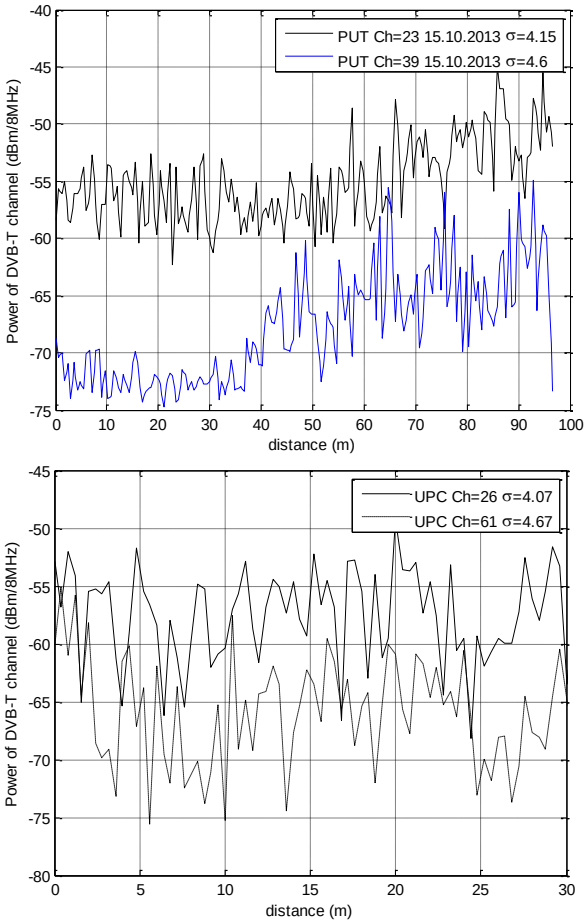

Fig. 4.4.7 Received power inside selected TV channel as a function of distance: in Poznan (upper plot) and in Barcelona (lower plot).

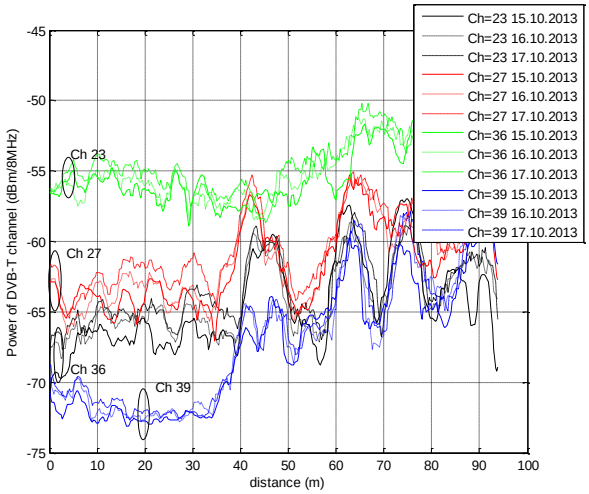

Fig. 4.4.8 Received power inside selected TV channel as a function of distance observed in various days

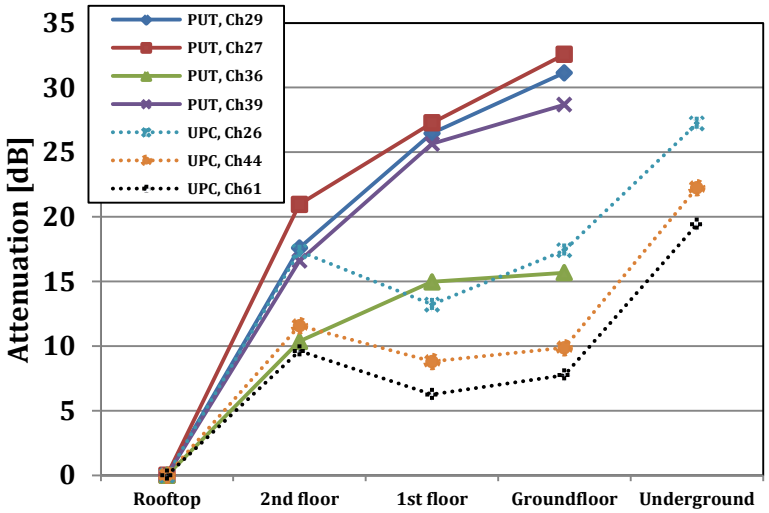

Fig. 4.4.9 Attenuation of the received signal power at different building levels relative to the power observed at the rooftop

4.4.2 Indoor REM database characteristics

4.4.2.1 Indoor REM database information

The REM should include all the relevant information needed to derive the transmit power limitations for any secondary transmitter (i.e. small cell) to be deployed in the building where the indoor REM applies or to modify the current transmission strategies by the secondary transmitters. Power limitations arise from the fact that the interference generated by the secondary transmitter to any DVB-T receivers should be below the acceptable limits not to degrade the TV reception capability.

Different works [12]-[14] have characterized the requirements for successful DVB-T reception. They are usually expressed in terms of the required Protection Ratio (*PR*). *PR* is defined as the minimum required ratio between the DVB-T signal and the interference at the DVB-T receiver input, i.e., it should be fulfilled that $P_r/I \geq PR$, where P_r is the received DVB-T signal and I is the total interference. *PR* is also sometimes referred to as rejection threshold of Desired to Undesired received power (D/U). The *PR* depends on whether the secondary transmits in the same channel as the DVB-T service and thus generates co-channel interference or whether it transmits in any of the adjacent channels. In the latter case, the *PR* should account for the selectivity characteristic of the DVB-T receiver and for the ACLR (Adjacent Channel Leakage Ratio) of the secondary transmitter that determines how much of the transmitted power is actually transmitted in the adjacent channel. In the context of this work we assume that the secondary transmitter is an LTE base station (small cell) and we take as a reference the required *PR* values that were obtained in [14] based on extensive measurements with different types of DVB-T receivers and LTE transmitters.

Under the above considerations, it is assumed that the indoor REM will contain a 3D characterisation of the radioelectrical propagation of the DVB-T signals inside the building as well as the required data to compute the maximum transmit powers. Specifically, the information to be stored can be classified as follows:

- Semi-static information: This corresponds to information elements that are not supposed to vary during secondary system operation, so that they can be acquired at some point of time and be

valid for a long period of time as long as regulatory conditions do not change (i.e. no new DVB-T licenses are assigned) nor new DVB-T transmitters appear. In particular, the following elements are considered:

- $P_r(\theta,N)$: Received power level of the DVB-T signal at each position $\theta=(x,y,z)$ inside the building for each TV channel N.
- $PR(i)$: Required protection ratio to ensure DVB-T reception in channel N when the secondary transmitter is working at channel $N+i$. Note that the case $i=0$ corresponds to the co-channel protection ratio while the case $i>0$ corresponds to the i-th adjacent channel protection ratio.
- $P_{r,min}$: Minimum received power level to ensure successful DVB-T reception.
- $L(d)$: Indoor propagation model to characterise the losses between any two points of the building as a function of the distance d and the building characteristics (e.g. number of floors, etc.).

- Dynamic information: This corresponds to information that needs to be updated dynamically depending on the operation of the secondary system. The following information is considered:
  - $P_{Tmax}(\theta,N)$: Maximum allowed transmit power for a secondary transmitter located at position $\theta=(x,y,z)$ and operating on TV channel N. This maximum power level will depend on the PR requirements of the DVB-T receivers and on the number and positions of the currently active secondary transmitters inside the building, in order to ensure that the aggregated interference that they generate is below the acceptable limits established by the PR. Correspondingly, this information needs to be updated every time that a new small cell is activated or deactivated in the considered building.

The focus of this study will be mainly placed on the acquisition of the received power levels $P_r(\theta,N)$ by means of measurements made with a certain granularity, as it will be discussed in section 4.7.2.3. Concerning PR and $P_{r,min}$ the values from [14] will be retained. As for the indoor propagation, the model from [15] is considered with the floor characteristics of the building. It is worth mentioning that the indoor propagation model could also be obtained based on measurements, but this is left for future work.

In order to compute the maximum allowed transmit power this work will focus on the worst case scenario in which the positions of the DVB-T receivers are unknown (e.g. in case of USB-stick DVB-T receivers connected to laptops that can be in any part of the building). However, in indoor scenarios other situations could also be considered in which e.g. the positions of the at least static DVB-T receivers could be registered in the database as well, or in which the only DVB-T reception point is the antenna at the rooftop.

A. Maximum allowed transmit power in the absence of other secondary transmitters

Assuming there is no other secondary transmitter in the building, the maximum allowed transmit power at point $\theta=(x,y,z)$ for a general channel $N+i$ needs to fulfil the following condition for any point θ' where a DVB-T receiver could be located:

$$\frac{P_r(\theta',N)}{\frac{P_{T\max}(\theta,N+i)}{L(\theta,\theta')}} \geq PR(i) \qquad (1)$$

where $L(\theta,\theta')$ denotes the propagation losses between the point θ where the secondary transmitter is located and the point θ' where the potential DVB-T receiver could be located. Based on this relationship the following distinction is done:

1) Co-channel secondary transmission (i=0)

In this case, it will be assumed that no secondary transmission is allowed at point θ if DVB-T reception is possible at this point (i.e. if $P_r(\theta,N)\geq P_{r,min}$). Though this condition would not be strictly necessary in theory as long as the protection ratio $PR(0)$ constraint is ensured when determining P_{Tmax}, in practice this would lead to very small values of transmit power that would actually prevent the secondary transmission. For this reason, we restrict secondary transmission to the points θ where DVB-T reception is not possible. In this case, the maximum transmit power is obtained from the most restrictive of the points θ' where DVB-T reception is possible. Then, from (1) it is obtained that:

$$P_{T\max}(\theta,N)=\begin{cases}0 & \text{if} \quad P_r(\theta,N)\geq P_{r\min}\\ \min\limits_{\theta' \text{ s.t. } P_r(\theta',N)\geq P_{r\min}}\left[\dfrac{P_r(\theta',N)\cdot L(\theta,\theta')}{PR(0)}\right] & \text{if} \quad P_r(\theta,N)<P_{r\min}\end{cases} \qquad (2)$$

2) Adjacent channel secondary transmission (i>0):

The main difference with the previous case is that now, since $PR(i)$ values are much lower than in the co-channel case, transmission in the adjacent channel $N+i$ can be considered even at a point where the DVB-T reception in channel N is possible. Then, from (1) the maximum transmit power is given by:

$$P_{T\max}(\theta,N+i)=\min_{\theta' \text{ s.t. } P_r(\theta',N)\geq P_{r\min}}\left[\frac{P_r(\theta',N)\cdot L(\theta,\theta')}{PR(i)}\right] \qquad (3)$$

For the case θ=θ' in which the secondary transmitter and the DVB-T receiver are located in the same position, it is assumed that in practice there will be always a minimum physical separation between the secondary transmitter and the DVB-T receiver [16], so $L(\theta',\theta)$ equals a minimum propagation loss L_{min} related with this physical separation.

B. Maximum allowed transmit power when there are other secondary transmitters

In case that a secondary transmitter already exists at a certain position θ^* operating in channel $N+i$ with power P_{Tsec} (where P_{Tsec} should be lower than $P_{Tmax}(\theta^*,N+i)$ computed from (2) and (3)), the maximum allowed power levels $P_{Tmax}(\theta,,N)$ stored in the REM need to account for the secondary interference already present in the building. In particular, if another transmitter had to be placed at position θ≠θ*, the following condition has to be fulfilled for any point θ' where the DVB-T receiver can be located:

$$\frac{P_r(\theta',N)}{\dfrac{P_{T\sec}}{L(\theta^*,\theta')}+\dfrac{P_{T\max}(\theta,N+i)}{L(\theta,\theta')}}\geq PR(i) \qquad (4)$$

Based on this expression, the maximum allowed transmit power can be formulated in a similar way as in (2) and (3):

1). Co-channel secondary transmission (i=0):

$$P_{T\max}(\theta,N)=\begin{cases}0 & \text{if} \quad P_r(\theta,N)\geq P_{r\min}\\ \min\limits_{\theta' \text{ s.t. } P_r(\theta',N)\geq P_{r\min}}\left[L(\theta,\theta')\left(\dfrac{P_r(\theta',N)}{PR(0)}-\dfrac{P_{T\sec}(\theta^*,N)}{L(\theta^*,\theta')}\right)\right] & \text{if} \quad P_r(\theta,N)<P_{r\min}\end{cases} \qquad (5)$$

2). Adjacent channel secondary transmission (i>0):

$$P_{T\max}(\theta, N+i) = \min_{\theta' \text{ s.t. } P_r(\theta',N)\geq P_{r\min}} \left[L(\theta,\theta') \left(\frac{P_r(\theta',N)}{PR(i)} - \frac{P_{T\sec}(\theta^*,N+i)}{L(\theta^*,\theta')} \right) \right] \quad (6)$$

Computations could easily be extended to consider the case with multiple existing secondary transmitters. Note in any case that the above computations assume that no modification is made in the transmit power level of the already existing secondary transmitter. Another possibility, left for future work, would be to perform an optimization process to jointly adjust the power of all the secondary transmitters whenever a new one has to be added.

It is worth mentioning that the analysis made in here assumes that there is sufficient isolation between different buildings to consider that a secondary transmitter located in one building does not interfere to DVB-T receivers in other buildings. While this is a simplification that needs to be further assessed with new measurements, it allows having a first estimation of the allowed transmit power levels and their feasibility to deploy indoor small cells.

4.4.2.2 Measurement location and set-up

The TVWS measurements to generate the indoor REM power levels $P_r(x,y,z,N)$ discussed in the previous section have been obtained in building D4 of the UPC Campus Nord in Barcelona. The location of this building is latitude: 41º 23' 20" N; longitude: 2º 6' 43" E; altitude: 175 m. A total of 21 DVB-T channels were detected at the rooftop. Although different channels were measured, for the sake of simplicity and to get a first insight on the potential allowed transmit power levels for secondary transmission, the results presented in this work focus only DVB-T channel 61 (794 MHz). The channel is received from a TV tower transmitter (named Torre de Collserola, see 0) located at 3.1 km with transmit power of 7.4 kW for this channel.

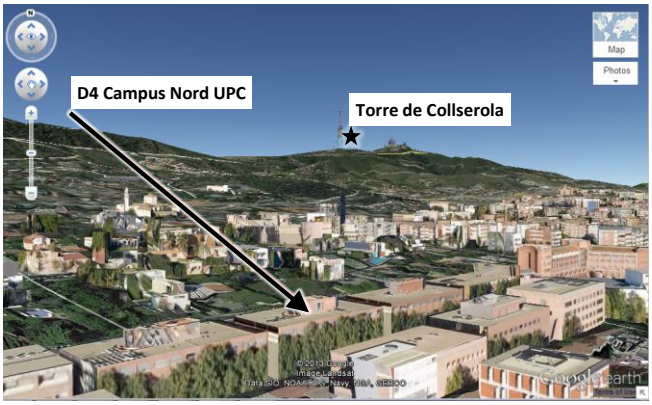

Fig. 4.4.10 Position of TV transmitter and the measured building.

The DVB-T signal has been measured by means of an omnidirectional antenna, then sent to a spectrum analyzer and finally stored on a portable computer via Matlab. The system setup is shown in 0.

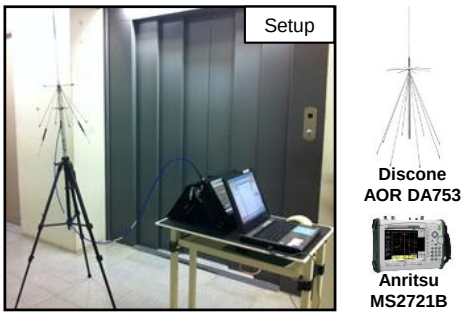

Fig. 4.4.11 Measurements system setup.

A passive discone antenna of type AOR DN753 was used, covering the frequency range from 75 to 3000MHz, and connected to ANRITSU MS2721B spectrum analyser. The resolution and video bandwidth of the spectrum analyzer are RBW=30kHz and VBW=100kHz, respectively.

4.4.2.3 Measurement analysis

First results of this section intend to analyse the required spatial granularity for the measurements stored in the indoor REM. For that purpose, multiple measurements have been performed in different positions inside the considered building. It is a four-level building with roughly 420 m^2 per floor (30m x 14m) including basement, ground floor, first and second floors. As an example, 0 shows the plan of the first floor where it can be observed how it is split in different offices/rooms. Measurements focus mainly in the interior part of the rooms where it can be envisaged that DVB-T receivers can be located, though some points in the corridors are also considered. Rooms are classified into small size offices (around 3m x 4m), medium size offices (e.g. those located in the four corners of 0) and large size rooms (e.g. laboratory D4-115 indicated in 0).

To assess the differences in received power inside the small size offices, initially 2 measurement points per office were considered located at two positions separated around 2 m, one located close to the window and the other close to the internal corridor. Table 7 presents the results in these two points for three offices indicated in 0. In each point a total of 50 measurements of the power level received in the 8MHz bandwidth of the DVB-T channel have been done. Presented results include the average and the standard deviation. Results in Table 7 reveal that the differences between the two points are relatively small, between 1 and 2 dB. Moreover, also low values of standard deviation can be observed.

Based on these observations, it was decided that one single point of measurement was sufficient for small size offices, while for large/medium size rooms measurements were made in more granularity, leading to the measurement points shown in 0 for the case of the first floor. Similar distributions of measurements were also made for the other floors.

Table 7 Measurements done in small offices at two points, one close to the window and the other close to the internal corridor

Office	Window Point		Corridor Point	
	Average (dBm)	StDev (dB)	Average (dBm)	StDev (dB)
D4-105	-60.54	0.73	-59.44	0.29
D4-106	-53.02	0.57	-54.30	0.98
D4-108	-60.45	0.94	-62.67	0.86

To assess the time stability of indoor measurements, the variation of the measured signal in specific points at different time instants was analysed. A first result in this respect is shown in Table 7, where the presented standard deviation for each point corresponds to a measurement duration of around 10min. The low values of standard deviation obtained, below 1 dB, suggest that a good stability is obtained for short term periods in the order of minutes. Moreover, in order to analyse the stability over long periods of time, measurements in some selected points were also repeated in different days and times. As an illustrative example of these measurements, in the case of the point inside laboratory D4-115 labelled A of 0, a total of 9 measurements done in 3 days and 3 different times of the day revealed that the standard deviation is only 2.11 dB. Consequently, it was considered that the time stability of the obtained measurements was sufficiently good so that measurements can be stored in an indoor REM. Similar observations in this respect where obtained in the prior work [JRAG-P2].

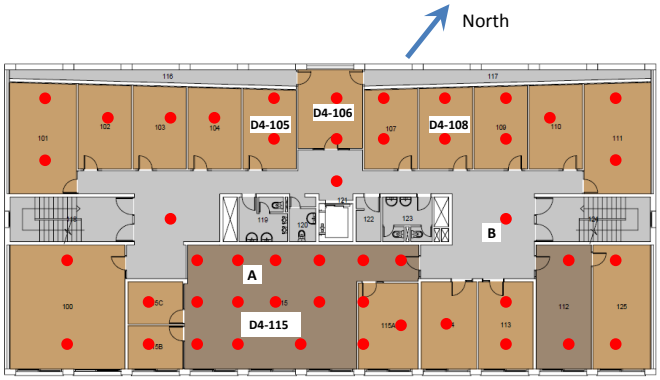

Fig. 4.4.12 First floor measurement points in the building.

Maximum Transmit Power when there is no other secondary transmitter

This subsection evaluates the dynamic information stored in the REM as indicated in section 4.7.2.1. In particular, it computes the maximum transmit power that can be allowed in the different points of the building assuming that there is no other active secondary transmitter. For that purpose, expressions (2) and (3) were used to determine P_{Tmax} for all the points of the building considering co-channel transmission in channel N=61 and adjacent channel transmission in N+1 and N+2.

The minimum received field strength to ensure successful reception of the DVB-T signal is assumed to be 56.7 dBμV/m [14], which corresponds to $P_{r,min}$= –80.5 dBm. The required protection ratios $PR(i)$ are obtained assuming two different types of receivers, namely an USB-Stick DVB-T receiver to be connected to PCs and laptops and a TV set with integrated digital tuner (IDTV) [14]. The indoor propagation losses are computed using the model adopted by FemtoForum and 3GPP TSG RAN4 [15] for communication between a terminal and a femtocell inside the same house. A frequency correction term to adapt the model to the TV band was introduced. Moreover, the minimum propagation loss existing between the secondary transmitter and any DVB-T receiver assuming that there will always be some physical separation between the two is assumed to be L_{min} =35 dB, that results from considering a distance of 2 m in the propagation model.

Focusing first on the possibility of having co-channel transmission in channel N=61, given that the building has direct line-of-sight and short distance with the TV tower transmitter, DVB-T reception is possible in most of the points inside the building, which prevents from the possibility of doing co-channel transmission in most of the cases. The only exceptions are a few points located at the basement, which is located below the street level. These points represent only 7.23% of the points in the building. Table 8 presents the P_{Tmax} statistics for these points according to (2) for the two

types of DVB-T receivers considered (USB stick and IDTV). It is observed that the maximum allowed transmit power takes actually very small values that would limit the coverage of the secondary transmitter to very few meters. In this respect it is not envisaged that these values could allow for the deployment of a small cell to provide satisfactory coverage in different parts of the building.

Table 8. P_{Tmax} for co-channel transmission in N=61

P_{Tmax}	USB Stick	IDTV
Min	-51.95 dBm	-50.95 dBm
Avg	-46.59 dBm	-45.59 dBm
Max	-39.50 dBm	-38.50 dBm

Concerning the secondary transmission in adjacent channels, 0 plots the Cumulative Distribution Function (CDF) of the maximum allowed transmit power P_{Tmax} according to (3) for the different points inside the building. Results are presented for both adjacent channels N+1 and N+2 and for both types of DVB-T receivers. As it can be observed, the allowed power levels are substantially higher than in the co-channel case, so it can be feasible the potential deployment of a small cell acting as a secondary transmitter. Specifically, when considering the USB-Stick DVB-T receiver, 90% of the points have a maximum allowed transmit power between −12 dBm and 9 dBm in the first adjacent channel, and between −10 dBm and 11 dBm in the second. Moreover, in half of the points the transmit power can be higher than −6 dBm in the first adjacent channel, which can be assumed a feasible level for successfully deploying an indoor small cell. For the IDTV receiver these values increase in around 2 dB.

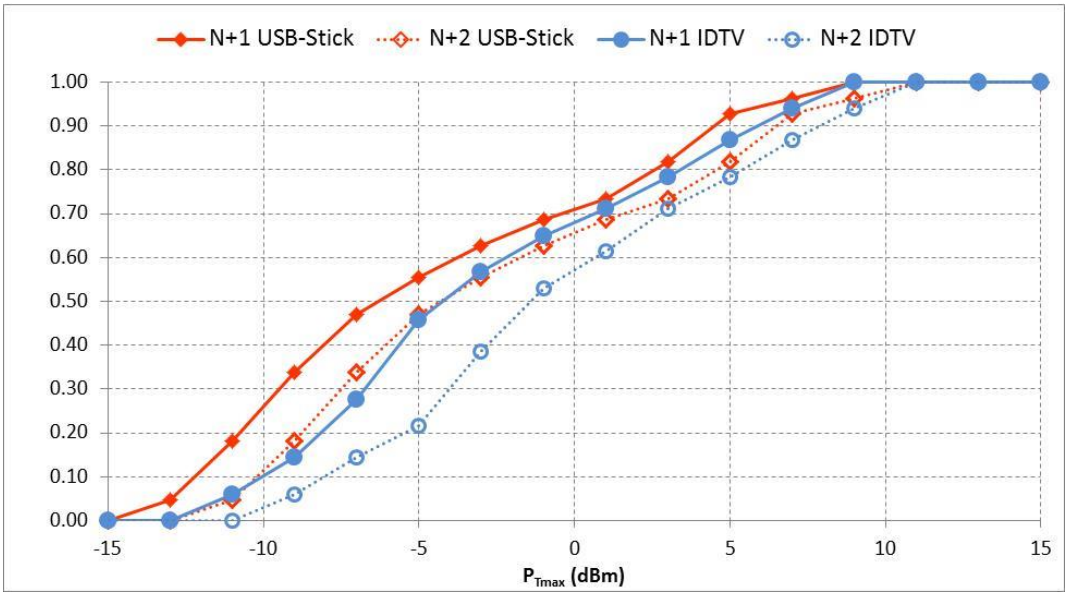

Fig. 4.4.13 CDF of the maximum transmit power P_{Tmax} for first and second adjacent channels

To gain insight on how the maximum power is distributed in different parts of the building, Table 9 presents different statistics of P_{Tmax} for different floors. Results are presented for the 1st adjacent channel and the USB stick receiver. In the case of the 1st floor measurements, positions have been further split between those lying in the northern and southern frontage sides (see 0) and between eastern and western sides. In that respect, the northern and eastern frontages have better visibility conditions with respect to the TV transmit tower than the western and southern

frontages. Therefore, it can be observed in the table that the maximum allowed power levels for the points located in the northern and eastern sides are larger than in the southern/western sides, because the DVB-T receiver at northern/eastern points has better signal conditions. It can also be noticed in the table that the maximum allowed transmit power tends to decrease when considering the ground floor and the basement.

Table 9. P_{Tmax} statistics for adjacent channel N+1 in the different floors

	Average (dBm)	5-th Percentile (dBm)	95-th Percentile (dBm)
Basement	-7.47	-13.61	0.15
Ground floor	-3.06	-10.94	5.70
1st floor (south side)	-9.15	-12.68	-4.48
1st floor (north side)	3.40	-0.21	8.95
1st floor (east side)	-3.20	-11.09	8.84
1st floor (west side)	-5.48	-12.68	3.72

Maximum Transmit Power when there is another secondary transmitter

This subsection analyses the case when there already exists a secondary transmitter in the building and the indoor REM has to be recomputed in order to determine the new maximum allowed power levels in each position according to (5)(6). Specifically, the existing secondary transmitter is assumed to be in the 1st floor at location labeled B (see 0). Considering adjacent channel *N*+1 and USB stick receiver, the maximum allowed transmit power at this location in order not to interfere with the DVB-T receivers would be –3.2 dBm. Accordingly, the transmit power of this secondary transmitter P_{Tsec} has been set to three possible values, namely –3.5 dBm, –5 dBm, –10 dBm. It is worth mentioning that the study only focuses on the interference that the secondary transmitters cause to the DVB-T receivers, so the mutual interference between secondary users is not taken into account. The considerations about this mutual interference are left for future work.

Under the abovementioned conditions, 0 plots the CDF of the new values for the maximum transmit power P_{Tmax} in the different positions inside the building for the above set of power levels and also for the case when there is no other secondary transmitter. It can be observed that P_{Tmax} values decrease when increasing the power P_{Tsec} of the secondary transmitter. However, only when P_{Tsec} is –3.5 dBm (i.e. very close to the maximum allowed power level of –3.2 dBm), significant differences are observed in the CDF. Differences are particularly noticeable for the largest values of P_{Tmax} which are between 2 and 3 dB less than when there is no other secondary transmitter.

The reason for such small differences is that the already existing secondary transmitter only has influence over a relatively small part of the building. To further analyse this fact, Table 10 presents the P_{Tmax} statistics in different parts of the building when the transmit power of the existing secondary transmitter is P_{Tsec}= –3.5 dBm. By comparing the results in Table 10 with those in Table 9 where no other secondary transmitter exists, it can be observed that the influence of the existing secondary transmitter in the first floor is negligible at the points in the ground floor and the basement. In turn, for the points in the first floor differences are particularly remarkable when

considering the points at the northern side (6 dB reduction in the 95-th percentile) and at the eastern side (10 dB reduction in the 95-th percentile) that correspond to the area closer to the position of the existing secondary transmitter (point B in 0). On the contrary, for the points in the southern and western sides differences are much smaller (in the order of 1.3 dB for the 95-th percentile).

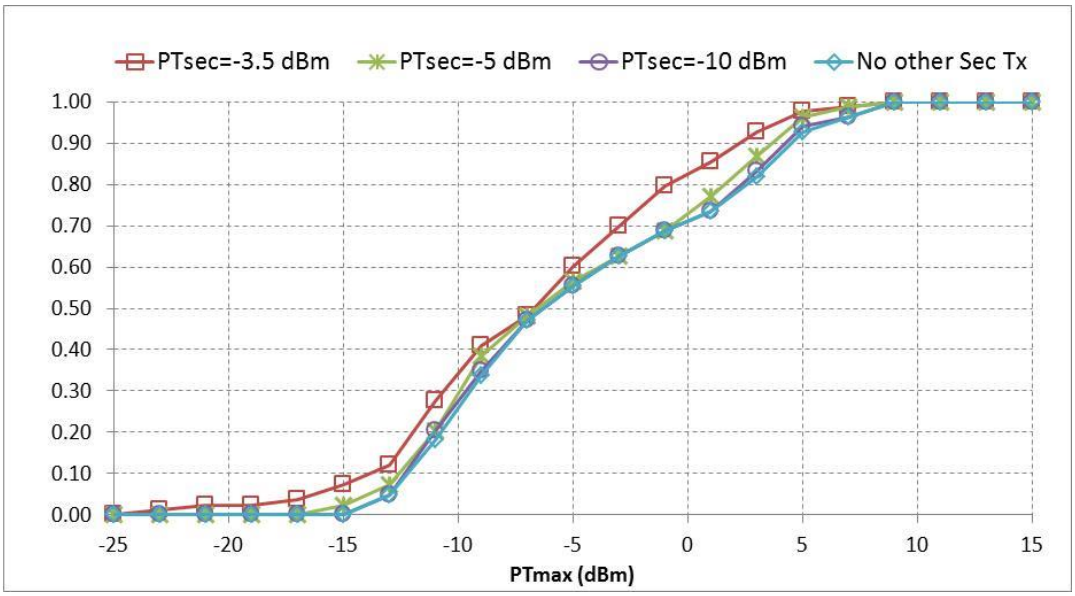

Fig. 4.4.13 CDF of the maximum transmit power P_{Tmax} for first adjacent channels when there is another secondary transmitter

Table 10. P_{Tmax} statistics for adjacent channel *N*+1in the different floors when there is another secondary transmitter in the 1st floor with P_{Tsec}=-3.5 dBm

	Average (dBm)	5-th Percentile (dBm)	95-th Percentile (dBm)
Basement	-7.47	-13.61	0.15
Ground floor	-3.06	-10.94	5.70
1st floor (south side)	-11.61	-20.71	-5.81
1st floor (north side)	-1.36	-5.58	2.88
1st floor (east side)	-9.87	-22.62	-1.25
1st floor (west side)	-5.91	-12.81	2.47

References

[1] A. Zalonis (Editor), “D13.1: Fundamental issues on energy- and bandwidth-efficient communications and networking”, Deliverable of the Newcom #, March 2014.

[2] J. Xiao, R. Q. Hu, Y. Qian, L. Gong, B. Wang ”Expanding LTE Network Spectrum with Cognitive Radios: From Concept to Implementation”, IEEE Wireless Communications, April, 2013, pp. 13-19

[3] J. Zander, L.K. Rasmussen, K.W. Song, P. Mähönen, M. Petrova, R. Jäntti, J. Kronander, ”On the scalability of Cognitive Radio: Assessing the Commercial Viability of Secondary Spectrum Access”, , IEEE Wireless Communications, April, 2013, pp.28-35

[4] T. Dudda, T. Irnich, ”Capacity of cellular networks deployed in TV White Space”, IEEE International Symposium on Dynamic Spectrum Access Networks, 2012.

[5] A. Achtzehn, M. Petrova, P. Mähönen, ”On the Performance of Cellular Network Deployments in TV Whitespaces”, IEEE ICC 2012.

[6] C.F. Silva, H. Alves, A. Gomes, ”Extension of LTE Operational Mode over TV White Spaces”, Future Network and Mobile Summit, 2011.

[7] J. W. Mwangoka, P. Marques, J. Rodriguez, ”Broker Based Secondary Spectrum Trading”, 6th International ICST Conference on Cognitive Radio Oriented Wireless Networks and Communications (CROWNCOM), 2011.

[8] M. Parzy, H. Bogucka, ”Policies and technology constraints for auctions in TV White Spaces - a practical approach for LTE-A”, International Symposium on Wireless Communication Systems (ISWCS),2012.

[9] F. Peng, Y. Gao, Y. Chen, K.K. Chai, L Cuthbert, ”Using TV White Space for Interference Mitigation in LTE Femtocell Networks”, IET International Conference on Communication Technology and Application (ICCTA), 2011.

[10] D3.3 “Control loops drive models & resource management assessment”, Deliverable D3.3 of the SACRA project, July, 2012.

[11] D5.2 ”Evaluation of Selected Measurement-based Techniques”, Deliverable of the FARAMIR project, February 2012.

[12] Advanced Television Systems Committee “ATSC Recommended Practice: Receiver Performance Guidelines (with Corrigendum No. 1 and Amendment No.1)”, Doc. A/74, November, 2007.

[13] G. L. Stüber, S. M. Almalfouh, D. Sale, “Interference Analysis of TV-Band Whitespace”, Proceedings of the IEEE, Vol. 97, No. 4, April, 2009, pp. 741-754.

[14] H. Aïache, et al. “Use-cases Analysis and TVWS Systems Requirements”, Deliverable D3.1 of the COGEU project, August, 2010.

[15] 3GPP TSG RAN WG4 Meeting #51: R4-092042 “Simulation assumptions and parameters for FDD HeNB RF requirements”, Alcatel-Lucent, May 2009.

[16] J. Lauterjung et al. “Spectrum measurements and anti-interference spectrum database specification”, Deliverable D4.1 of the COGEU project, October, 2010.

Comments and suggestions for the improvement of this document are most welcome and should be sent to:

project_office@newcom-project.eu

---

http://www.newcom-project.eu